International Journal of Physical Sciences

Volume 8 Number 28 30 July, 2013

ISSN 1992-1950

Academic Journals

ABOUT IJPS

The **International Journal of Physical Sciences (IJPS)** is published weekly (one volume per year) by Academic Journals.

International Journal of Physical Sciences (IJPS) is an open access journal that publishes high-quality solicited and unsolicited articles, in English, in all Physics and chemistry including artificial intelligence, neural processing, nuclear and particle physics, geophysics, physics in medicine and biology, plasma physics, semiconductor science and technology, wireless and optical communications, materials science, energy and fuels, environmental science and technology, combinatorial chemistry, natural products, molecular therapeutics, geochemistry, cement and concrete research, metallurgy, crystallography and computer-aided materials design. All articles published in IJPS are peer-reviewed.

Submission of Manuscript

Submit manuscripts as e-mail attachment to the Editorial Office at: ijps@academicjournals.org. A manuscript number will be mailed to the corresponding author shortly after submission.

For all other correspondence that cannot be sent by e-mail, please contact the editorial office (at ijps@academicjournals.org).

The International Journal of Physical Sciences will only accept manuscripts submitted as e-mail attachments.

Please read the **Instructions for Authors** before submitting your manuscript. The manuscript files should be given the last name of the first author.

Editors

Editorial Board

Instructions for Author

Electronic submission of manuscripts is strongly encouraged, provided that the text, tables, and figures are included in a single Microsoft Word file (preferably in Arial font).

The **cover letter** should include the corresponding author's full address and telephone/fax numbers and should be in an e-mail message sent to the Editor, with the file, whose name should begin with the first author's surname, as an attachment.

Article Types

Three types of manuscripts may be submitted:

Regular articles: These should describe new and carefully confirmed findings, and experimental procedures should be given in sufficient detail for others to verify the work. The length of a full paper should be the minimum required to describe and interpret the work clearly.

Short Communications: A Short Communication is suitable for recording the results of complete small investigations or giving details of new models or hypotheses, innovative methods, techniques or apparatus. The style of main sections need not conform to that of full-length papers. Short communications are 2 to 4 printed pages (about 6 to 12 manuscript pages) in length.

Reviews: Submissions of reviews and perspectives covering topics of current interest are welcome and encouraged. Reviews should be concise and no longer than 4-6 printed pages (about 12 to 18 manuscript pages). Reviews are also peer-reviewed.

Review Process

All manuscripts are reviewed by an editor and members of the Editorial Board or qualified outside reviewers. Authors cannot nominate reviewers. Only reviewers randomly selected from our database with specialization in the subject area will be contacted to evaluate the manuscripts. The process will be blind review.

Decisions will be made as rapidly as possible, and the journal strives to return reviewers' comments to authors as fast as possible. The editorial board will re-review manuscripts that are accepted pending revision. It is the goal of the IJPS to publish manuscripts within weeks after submission.

Regular articles

All portions of the manuscript must be typed double-spaced and all pages numbered starting from the title page.

The Title should be a brief phrase describing the contents of the paper. The Title Page should include the authors' full names and affiliations, the name of the corresponding author along with phone, fax and E-mail information. Present addresses of authors should appear as a footnote.

The Abstract should be informative and completely self-explanatory, briefly present the topic, state the scope of the experiments, indicate significant data, and point out major findings and conclusions. The Abstract should be 100 to 200 words in length.. Complete sentences, active verbs, and the third person should be used, and the abstract should be written in the past tense. Standard nomenclature should be used and abbreviations should be avoided. No literature should be cited.

Following the abstract, about 3 to 10 key words that will provide indexing references should be listed.

A list of non-standard **Abbreviations** should be added. In general, non-standard abbreviations should be used only when the full term is very long and used often. Each abbreviation should be spelled out and introduced in parentheses the first time it is used in the text. Only recommended SI units should be used. Authors should use the solidus presentation (mg/ml). Standard abbreviations (such as ATP and DNA) need not be defined.

The Introduction should provide a clear statement of the problem, the relevant literature on the subject, and the proposed approach or solution. It should be understandable to colleagues from a broad range of scientific disciplines.

Materials and methods should be complete enough to allow experiments to be reproduced. However, only truly new procedures should be described in detail; previously published procedures should be cited, and important modifications of published procedures should be mentioned briefly. Capitalize trade names and include the manufacturer's name and address. Subheadings should be used. Methods in general use need not be described in detail.

Results should be presented with clarity and precision. The results should be written in the past tense when describing findings in the authors' experiments. Previously published findings should be written in the present tense. Results should be explained, but largely without referring to the literature. Discussion, speculation and detailed interpretation of data should not be included in the Results but should be put into the Discussion section.

The Discussion should interpret the findings in view of the results obtained in this and in past studies on this topic. State the conclusions in a few sentences at the end of the paper. The Results and Discussion sections can include subheadings, and when appropriate, both sections can be combined.

The Acknowledgments of people, grants, funds, etc should be brief.

Tables should be kept to a minimum and be designed to be as simple as possible. Tables are to be typed double-spaced throughout, including headings and footnotes. Each table should be on a separate page, numbered consecutively in Arabic numerals and supplied with a heading and a legend. Tables should be self-explanatory without reference to the text. The details of the methods used in the experiments should preferably be described in the legend instead of in the text. The same data should not be presented in both table and graph form or repeated in the text.

Figure legends should be typed in numerical order on a separate sheet. Graphics should be prepared using applications capable of generating high resolution GIF, TIFF, JPEG or Powerpoint before pasting in the Microsoft Word manuscript file. Tables should be prepared in Microsoft Word. Use Arabic numerals to designate figures and upper case letters for their parts (Figure 1). Begin each legend with a title and include sufficient description so that the figure is understandable without reading the text of the manuscript. Information given in legends should not be repeated in the text.

References: In the text, a reference identified by means of an author‘s name should be followed by the date of the reference in parentheses. When there are more than two authors, only the first author‘s name should be mentioned, followed by ’et al‘. In the event that an author cited has had two or more works published during the same year, the reference, both in the text and in the reference list, should be identified by a lower case letter like ’a‘ and ’b‘ after the date to distinguish the works.

Examples:

Abayomi (2000), Agindotan et al. (2003), (Kelebeni, 1983), (Usman and Smith, 1992), (Chege, 1998; 1987a,b; Tijani, 1993,1995), (Kumasi et al., 2001)

References should be listed at the end of the paper in alphabetical order. Articles in preparation or articles submitted for publication, unpublished observations, personal communications, etc. should not be included in the reference list but should only be mentioned in the article text (e.g., A. Kingori, University of Nairobi, Kenya, personal communication). Journal names are abbreviated according to Chemical Abstracts. Authors are fully responsible for the accuracy of the references.

Examples:

Ogunseitan OA (1998). Protein method for investigating mercuric reductase gene expression in aquatic environments. Appl. Environ. Microbiol. 64:695-702.

Gueye M, Ndoye I, Dianda M, Danso SKA, Dreyfus B (1997). Active N2 fixation in several Faidherbia albida provenances. Ar. Soil Res. Rehabil. 11:63-70.

Charnley AK (1992). Mechanisms of fungal pathogenesis in insects with particular reference to locusts. In: Lomer CJ, Prior C (eds) Biological Controls of Locusts and Grasshoppers: Proceedings of an international workshop held at Cotonou, Benin. Oxford: CAB International, pp 181-190.

Mundree SG, Farrant JM (2000). Some physiological and molecular insights into the mechanisms of desiccation tolerance in the resurrection plant Xerophyta viscasa Baker. In Cherry et al. (eds) Plant tolerance to abiotic stresses in Agriculture: Role of Genetic Engineering, Kluwer Academic Publishers, Netherlands, pp 201-222.

Short Communications

Short Communications are limited to a maximum of two figures and one table. They should present a complete study that is more limited in scope than is found in full-length papers. The items of manuscript preparation listed above apply to Short Communications with the following differences: (1) Abstracts are limited to 100 words; (2) instead of a separate Materials and Methods section, experimental procedures may be incorporated into Figure Legends and Table footnotes; (3) Results and Discussion should be combined into a single section.

Proofs and Reprints: Electronic proofs will be sent (e-mail attachment) to the corresponding author as a PDF file. Page proofs are considered to be the final version of the manuscript. With the exception of typographical or minor clerical errors, no changes will be made in the manuscript at the proof stage.

International Journal of Physical Sciences

Table of Contents: Volume 8 Number 28 30 July, 2013

ARTICLES

academicJournals

Vol. 8(28), pp. 1442-1457, 30 July, 2013
DOI: 10.5897/IJPS10.544
ISSN 1992 - 1950 © 2013 Academic Journals
http://www.academicjournals.org/IJPS

International Journal of Physical Sciences

Full Length Research Paper

Study of the effect of particles size and volume fraction concentration on the thermal conductivity and thermal diffusivity of Al_2O_3 nanofluids

Faris Mohammed Ali, W. Mahmood Mat Yunus* and Zainal Abidin Talib

Department of Physics, University Putra Malaysia, 43400 UPM, Serdang, Selangor, Malaysia.

Accepted 29 July, 2013

In this study we present new data for the thermal conductivity enhancement in four nanofluids containing 11, 25, 50, and 63 nm diameter Aluminum oxide (Al_2O_3) nanoparticles in distilled water. The nanofluids were prepared using single step method (that is, by dispersing nanoparticle directly in base fluid) which was gathered in ultrasonic device for approximately 7 h. The transient hot-wire laser beam displacement technique was used to measure the thermal conductivity and thermal diffusivity of the prepared nanofluids. The thermal conductivity and thermal diffusivity were obtained by fitting the experimental data to the numerical data simulated for Al_2O_3 in distilled water. The results show that, the thermal conductivity and thermal diffusivity enhancement of nanofluids increases as the particle size increases. Thermal conductivity and thermal diffusivity enhancement of Al_2O_3 nanofluids was increase as the volume fraction concentration increases. This enhancement attributed to the many factors such as, ballistic energy, nature of heat transport in nanoparticle, and interfacial layer between solid/fluids.

Key words: Thermal conductivity, thermal diffusivity, effect of particle size, effect of volume fraction.

INTRODUCTION

Nanofluids are defined as the dispersed of solid nanoparticles (metal or metal oxide) in the fluid. Nanofluids have attracted much attention recently because of their potential as high performance heat transfer fluids in electronic cooling and automotive (Wen and Ding, 2006; Maiga et al., 2006). This interest begins with the work of Eastman et al. (1997); Lee et al. (1999); and Wang et al. (1999). They have reported the thermal conductivity enhancements of common heat transfer fluids such as ethylene glycol, water, oil, and small addition of solid nanoparticles. For example, Eastman has showed that, the enhancement of the thermal conductivity of Copper (Cu) nanoparticle suspension in ethylene glycol increases by 40% at volume fraction concentration of 0.3% (Eastman et al., 1997). Similarly, Choi and his co-researchers has illustrated that, the enhancement in the thermal conductivity of carbon nanotubes (NCT) suspension in oil was 160% measured at volume fraction concentration of 1% (Choi et al., 2001).

The effects of particle size, volume fraction, and temperature on thermal conductivity have been investigated by Michael et al. (2009a). They used a liquid metal transient hot wire device to measure the thermal conductivity of alumina dispersed in water, ethylene glycol, and ethylene glycol-water mixtures base fluids. The measurements have been carried out at a specific concentration and temperature, with an error of ± 2%. The results showed that, the thermal conductivity as a function of temperature was close to the value of base fluids. However, the maximum enhancement of thermal conductivity appeared at 400K and 380K, respectively. In general their results showed that, the thermal

*Corresponding author. E-mail: wmmyunus@gmail.com.

conductivity enhancement of alumina nanofluids at room temperature decreased as the particle size decreases, but increased with volume fraction concentration. The effect of particle size on the effective thermal conductivity of Al_2O_3 suspension in water nanofluids have been investigated using steady-state method (Calvin and Peterson, 2007). The nanoparticle with 36 and 47 nm were dispersed in water base fluid at different volume fraction ranging from 0.5 to 6%. The measurements were carried out for a temperature range of 27 to 37°C. They found out that, the enhancement in thermal conductivity of two types of nanofluids (36 and 47 nm) increased nonlinearly with volume fraction and temperature. The most significant finding was that, the largest enhancement was occurred at a temperature of approximately 32°C for volume fraction ranging from 2 to 4%.

The effect of particle size on some thermophysical properties such as thermal conductivity and viscosity of the nanofluids have been studied experimentally using a transient hot wire method and numerically studied using a simplified molecular dynamics method (Wen and Qing, 2008). In this case, the Aluminum oxide (Al_2O_3) nanoparticle with particle sizes of 35, 45, and 90 nm were suspended in water and ethylene glycol at different volume fraction concentrations were studied. The results showed a good agreement between the experimental data and numerical results. According to the numerical results, increasing the volume fraction concentration or decreasing the particle size of nanoparticle could increase the thermal conductivity of nanofluids. This is due to the increasing of viscosity of the nanofluid. For suitable particle size and volume fraction, the increasing of viscosity gives an enhancement of heat transfer capability.

The effect of particle size on the thermal conductivity of alumina Al_2O_3 nanoparticle suspension in water and ethylene glycol base fluids for particle size ranging from 8 to 282 nm have been conducted by Michael et al. (2009b). The thermal conductivity of the nanofluid was measured using a transient hot wire technique. The results show that, the enhancement in thermal conductivity of nanofluids increases with the increasing of particle size. They also developed the correlation between thermal conductivity enhancements with particle size.

The thermal conductivity of titanium dioxide, zinc-oxide, and alumina dispersed in water and ethylene glycol as base fluids have been measured using the transient hot-wire method (Kim et al., 2007). In this study, the effect of particle size and laser irradiation has been investigated. Emphasis was placed on the effect of particle size suspension in base fluid on the enhancement thermal conductivity. Also, the effect of laser pulse irradiation, which means, the changing of the particle size by laser ablation, was tested only for ZnO nanofluids. The results show that, the enhancement thermal conductivity of nanofluids increases linearly with decreasing the particle size, but no existing empirical or theoretical correlation can explain this behavior. In addition, the results illustrated that, high power laser irradiation can lead to substantial enhancement in the effective thermal conductivity although only a small volume fraction concentration of the nanoparticles are fragmented. However, the results show that, the thermal conductivity of the nanofluids increases linearly with the volume fraction concentration for Al_2O_3, ZnO, and TiO_2 nanofluids. Generally, the enhancement in the thermal conductivity that were observed in the approximately range of 15 to 25% were relative to the base fluid. The maximum enhancement was observed when the smallest nanoparticle size (10 nm) was suspended in ethylene glycol. The measurements of thermal conductivity of nanofluids using Transient Hot-Wire method was recently reported by Walvekar et al. (2012) and Pang and Kang (2012). They have carried out the investigation of the effect of particle volume fraction and the concenration of stabilizing agent as well as the fluid temperature on the thermal conductivity of NCT nanofluid. Their results show that, the thermal conductivity of the sample increases with the increasing of concentration of CNT, stabilizing agent, and temperature.

In the present study, we report measurements of the thermal conductivity and thermal diffusivity of Al_2O_3 nanofluids using transient hot-wire laser beam displacement technique. Four different particle sizes of nanofluid were studied in order to investigate the effect of particle size on the thermal conductivity and thermal diffusivity enhancement. The transient hot-wire laser beam displacement technique was chosen with two reasons; first we can obtained the thermal conductivity and thermal diffusivity values from a single measurement; secondly, we can simply eliminate the experiment error due to the convection process in liquid.

MATERIALS AND METHODS

Preparation of nanofluids

The Al_2O_3 nanoparticles with average particle sizes of 11, 25, 50, and 63 nm were purchased from Nanostructured and Amorphous Materials, Inc. USA. The nanofluid samples were prepared using the one-step method, similar to the one reported by Choi (1998). The Al_2O_3 nanoparticles were suspended in the distilled water base fluid to produce 5 different volume fraction concentrations (0.225, 0.55, 0.845, 1.124, and 1.4%) samples. The nanoparticles and base fluid were mixed and kept in an ultrasonic bath for more than 7 h. Acetyl trimethyl ammonium bromide (CTAB) was added as a surfactant for the mixtures. The size and the particle distribution of the nanoparticles in base fluids were verified and measured using TEM (Hitachi 7100 TEM).

Experimental setup

The experimental setup is based on the Transient Hot-Wire-laser beam displacement technique. It consists of a heating a wire, a CW He-Ne laser, as the probe beam, a lens with a focal length of 50

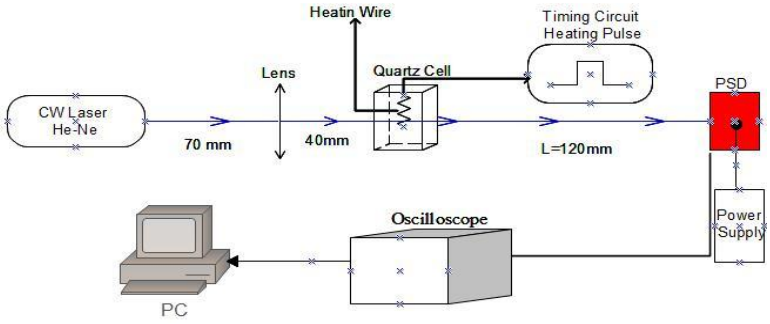

Figure 1. Schematic diagram of the hot wire-laser probe beam displacement technique

mm and a quartz cell as the nanofluids container. A position sensitive detector (PSD) was used to collect the signal of the deflected laser beam. The beam deflection signal was monitored using a Lecroy 9310A Digital Oscilloscope. Figure 1 shows the schematic diagram of the set up. A CW He-Ne laser operated at 632.8 nm with an output power of 2 mW serves as the probe beam. The measurements were carried out using the nanofluid quartz cell with the light path of 10.5 mm. The heating wire diameter and resistance was measured to be 254 μm and 2.38 Ω/cm, respectively. The wire was positioned vertically and perpendicular to the probe beam. A home-made timing circuit was used to control the heating current through the resistance wire to provide a pulse heating source. The heating pulse was 0.35 s with a heating voltage of 5 volts.

Thermal and laser beam displacement models

The purpose of a thermal model is to derive the fundamental correlations for conduction heat transfer performance analysis of the nanofluid, which is considered as a single phase fluid in the conventional approach (Yimin and Wilfried, 2000). A thermal model of heat conduction with guess values of k_{nf} and α_{nf} needs to be established first to solve the temperature distribution within the test liquid. Then the temperature profile of the laser probe beam deflection can be determined by relating the deflection angle with the solved temperature gradient through a beam deflection model (Jonathan et al., 1990). The heat conduction equations in the wire, fluid and nanoparticles are established using the cylindrical coordinate system in dimensionless forms as shown in Equations 1, 2, and 3, respectively.

$$\gamma_1 \frac{\partial u_w(r,\tau)}{\partial \tau} = \frac{\partial^2 u_w(r,\tau)}{\partial r^2} + \frac{1}{r}\frac{\partial u_w(r,\tau)}{\partial r} + g(r,\tau) \quad (1)$$

$$\gamma_2 \frac{\partial u_f(r,\tau)}{\partial \tau} = \frac{\partial^2 u_f(r,\tau)}{\partial r^2} + \frac{1}{r}\frac{\partial u_f(r,\tau)}{\partial r} \quad (2)$$

$$\gamma_3 \frac{\partial u_{np}(r,\tau)}{\partial \tau} = \frac{\partial^2 u_{np}(r,\tau)}{\partial r^2} + \frac{1}{r}\frac{\partial u_{np}(r,\tau)}{\partial r} \quad (3)$$

Where τ is the dimensionless time constant, u is the dimensionless temperature and γ is the dimensionless variable.

In a conventional approach, it is assumed that, both the liquid and particle phases are in thermal equilibrium and flow at the same velocity, therefore, the nanofluids behaved like a common pure fluid. This implies that, the whole equation of a single-phase fluid has been applied directly to the nanofluids (Wongwises and Weerapun, 2007). As the thermal and flow equilibrium between the fluid phase and nanoparticles, a uniform shape and size for nanoparticles becomes the most important parameter to be considered for enhancement in the thermal conductivity and thermal diffusivity of the nanofluid (Yimin and Wilfried, 2000; Calvin and Peterson, 2010; Omid and Ahmad, 2009). Therefore, we get:

$$\frac{\partial u_f(r,\tau)}{\partial \tau} \cong \frac{\partial u_{np}(r,\tau)}{\partial \tau} \quad (4)$$

$$\frac{\partial u_f(r,\tau)}{\partial r} \cong \frac{\partial u_{np}(r,\tau)}{\partial r} \quad and \quad \frac{\partial^2 u_f(r,\tau)}{\partial r^2} \cong \frac{\partial^2 u_{np}(r,\tau)}{\partial r^2} \quad (5)$$

For this reason, we can say that Equation 2 is approximately equal to Equation 3 so the dimensionless heat conduction equations of a single-phase fluid and nanoparticles becomes:

$$\gamma_{nf} \frac{\partial u_{nf}(r,\tau)}{\partial \tau} = \frac{\partial^2 u_{nf}(r,\tau)}{\partial r^2} + \frac{1}{r}\frac{\partial u_{nf}(r,\tau)}{\partial r} \quad (6)$$

The dimensionless boundary conditions are written as:

$$\left.\frac{\partial u(r,t)}{\partial r}\right|_{r=0} = 0 \quad (7)$$

$$k_{12} \left.\frac{\partial u(r,t)}{\partial r}\right|_{\substack{r\to 1 \\ r\langle 1}} = \left.\frac{\partial u(r,t)}{\partial r}\right|_{\substack{r\to 1 \\ r\rangle 1}} \quad (8)$$

$$u(r,t)\big|_{\substack{r=1 \\ r\langle 1}} = u(r,t)\big|_{\substack{r=1 \\ r\rangle 1}} \quad (9)$$

$$u(r,t)\big|_{r\to\infty} \to 1 \quad (10)$$

With the dimensionless initial condition given as;

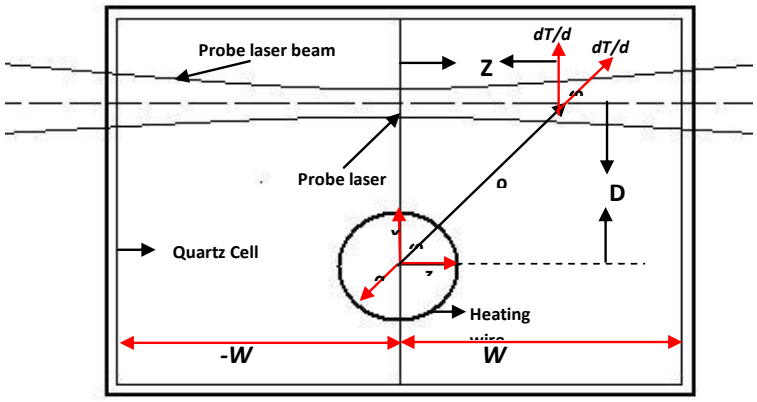

Figure 2. Geometry of heating wire and probe laser beam.

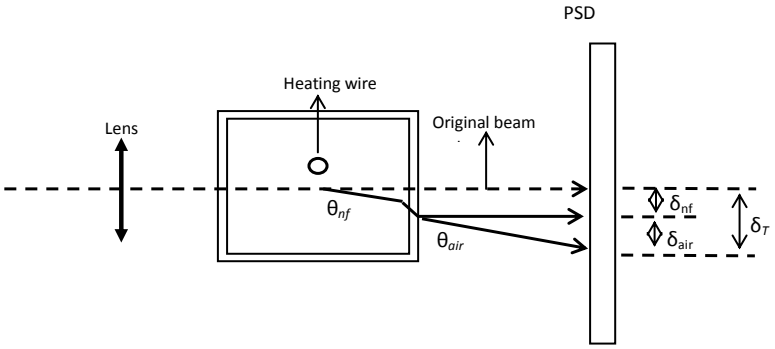

Figure 3. Optical path of probe laser beam.

$$u(r,0)=1 \tag{11}$$

and

$$\gamma_1=\frac{a^2}{\alpha_1 t_p},\qquad \gamma_{nf}=\frac{a^2}{\alpha_2 t_p},\qquad k_{12}=\frac{k_1}{k_{nf}} \tag{12}$$

Where t_p is the heating pulse duration; a is the radius of the wire, and k and α are thermal conductivity and thermal diffusivity respectively.

The volumetric heat generation $g(r,\tau)$ rate equation in dimensionless form is:

$$g(r,\tau)=\begin{cases}\dfrac{VI}{\pi T_0 k_1 l} & r \le l,\ \ \tau \le \tau_0\\ 0 & \text{r} \rangle \text{l},\ \ \tau \rangle \tau_0\end{cases} \tag{13}$$

Where V and I are the voltage and current of heating wire respectively.

The beam deflection angle equation in the nanofluid caused by gradient of temperature (θ) can be expressed as:

$$\theta_{nf}=\int_0^{L_f}\frac{\nabla n\cdot\vec{a}_x}{n}dz=\frac{1}{n_0}\int_0^{L_f}(\nabla n\cdot\vec{a}_x)dz \tag{14}$$

Where n is the nanofluid refractive index , L_{nf} is the probe beam path length in nanofluid , $\vec{a}_x$ is the spatial unit vector perpendicular to the original probe beam, z is the spatial direction parallel to the original beam path and n_o is the normal value and can be ignored from the integral in Equation 14. The refractive index is a function of temperature; therefore the refractive index gradient and the temperature gradient can be related to each other by the equation:

$$\nabla n=\frac{dn}{dT}\nabla T \tag{15}$$

In order to derive the beam deflection position on the detector, we consider the sample cell geometry and the beam deflection as shown in Figures 2 and 3 respectively. From Figure 2 we can write Equation 14 in term of cell geometry as:

$$\theta_{nf}=\frac{1}{n}\frac{dn}{dT}\int_{-W}^{W}\frac{D}{\sqrt{D^2+Z^2}}.\frac{dT}{d\rho}dz \tag{16}$$

Where D is the distance between the heating wire and probe beam,

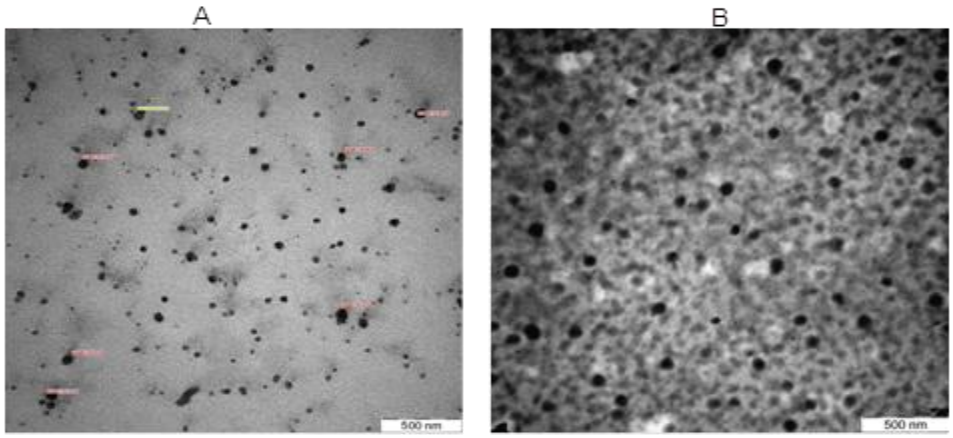

Figure 4. TEM image of Al2O3 (50 nm) nanoparticles dispersed in water after 7 h sonication, (a) volume fraction concentration 1.4% (b) volume fraction concentration 1.124%.

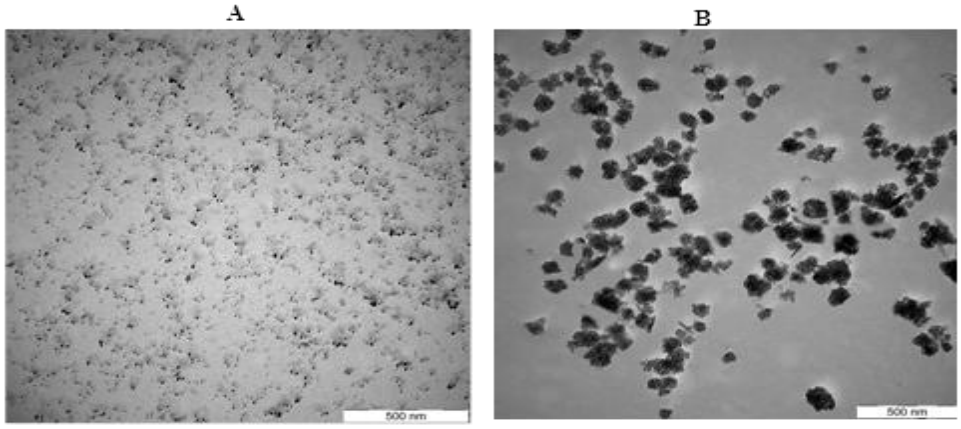

Figure 5. TEM image of Al_2O_3 (11 nm) nanoparticles dispersed in water after 7 h sonication, (a) volume fraction concentration 1.4% (b) volume fraction concentration 1.124%.

W the inner distant of the cell region within which the probe beam deflected as shown in Figure 2. Thus, the probe beam deflection angle in the nanofluid depends on the temperature gradient *dT/dρ* which can be obtained by solving the transient heat conduction equation in the heating wire and nanofluid numerically as discussed above. Therefore, the total beam deflection (δ_T , in Figure 3) on position sensitive detector (PSD) is the sum of the beam deflection in the nanofluid (δ_{nf}) and in air (δ_{air}) as shown in Figure 3, which can be expressed as:

$$\delta_T^n = \frac{w - W + n_o L_{air}}{n_o} \frac{dn}{dT} \frac{T_o}{a} \frac{\Delta z}{2} \sum_{i=0}^{N_Z} \frac{D}{\sqrt{D^2 + Z_{i+1}^2}} \frac{du_{nf,i+1}^n}{dr} + \frac{D}{\sqrt{D^2 + Z_i^2}} \frac{du_{nf,i}^n}{dr} \quad (17)$$

Where *W* is the half width of the quartz cell, T_o Initial temperature, Δz is the grid spacing along z-axis and L_{air} is the probe beam path length in the air. The non-dimensional term, *du/dr* is related to the temperature distribution as:

$$\frac{du}{dr} = \frac{a}{T_o} \frac{dT}{d\rho} \quad (18)$$

The numerical data were obtained by solving the transient heat conduction equations of the heating wire and the nanofluid medium using the finite difference Method based on Crank-Nicolson algorithm. Thermal conductivity and thermal diffusivity of Al_2O_3 nanofluids were simultaneously obtained by fitting the experimental data to the generated numerical data for different particle size of nanofluids (11, 25, and 50 nm) samples.

RESULTS AND DISCUSSION

Figures 4 and 5 show the TEM images of nanoparticle distribution of Al_2O_3 nanoparticles in the base distilled water fluids after 6 h in the sonication process. The images show that, the Al_2O_3 nanoparticles were

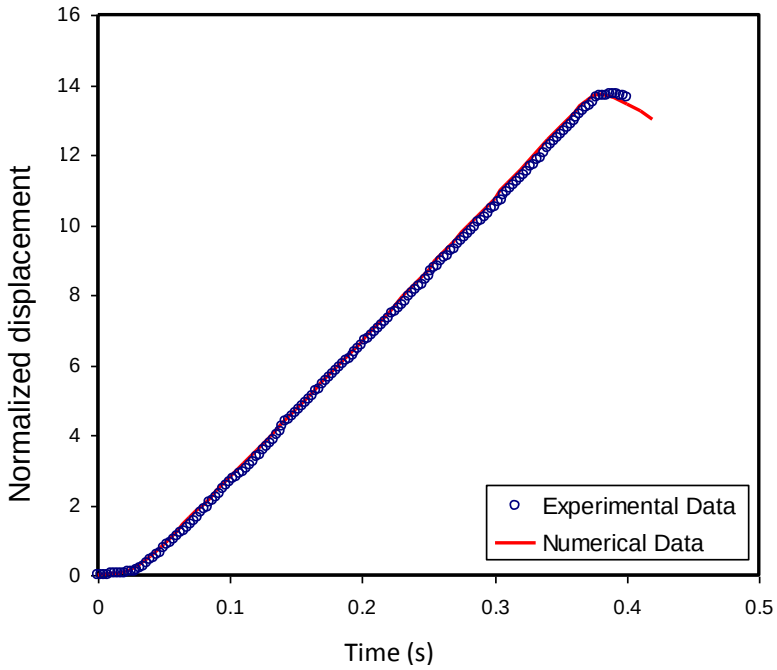

Figure 6. Normalized probe laser beam displacement for Al_2O_3 (50 nm) in water at D = 300 µm.

aggregated to form nanoparticle clusters and evenly distributed in the base fluids. These showed that, the nanoparticles are in nano-metric scale around (14 to 70 nm) and are semi-spherical in shape. The measurement of thermal diffusivity and the thermal conductivity is based on the energy equation for heat conduction and the deflection of the laser probe beam.

Figure 6 shows a typical plot of normalized displacement signal as a function of time for Al_2O_3 (50 nm) in water measured at D = 300 µm. The thermal conductivity and thermal diffusivity of were simultaneously obtained by fitting the experimental data to the numerical values calculated using Equation 17. The best value was recorded when the smallest total error between the numerical data and the experimental data was obtained that is:

$$\varepsilon = \sum_{j=0}^{N} (v_{exp} - v_{model})^2 \quad (19)$$

Where v_{exp} and v_{model}, are the experimental and numerical model values of the normalized position, sensitive detector output voltage, respectively.

The results of the thermal conductivity and thermal diffusivity of Al_2O_3 (11 nm) nanoparticles suspension in distilled water were 0.646, 0.655, 0.661, 0.669, 0.676 W/m.K, and (1.5758, 1.6219, 1.6457, 1.6738, 1.7270) × 10^{-7} m^2/s at volume fraction concentrations of 0.225, 0.55, 0.845, 1.124 and 1.4%, respectively. Obviously, the thermal conductivity and thermal diffusivity of Al_2O_3 (63 nm) were higher than thermal conductivities and thermal diffusivities of Al_2O_3 with particle sizes of 11, 25, and 50 nm. Table 1 shows the thermal conductivity and thermal diffusivities of Al_2O_3 nanoparticles suspension in distilled water at different particle size and different volume fraction concentration. These results showed that, the thermal conductivity and thermal diffusivity of Al_2O_3 increased with the increasing of particle size and volume fraction.

Effect of particle size on thermal properties of nanofluids

The thermal conductivity and diffusivity of nanofluids measured at different volume fractions from 1.4 to 0.225% and particle sizes ranging from 11 to 63 nm are presented in Table 1 and Figures 7 to 16. All measurements were made at room temperature with the hot wire-laser probe beam displacement technique. The samples consisted of Al_2O_3 nanoparticles dispersed in distilled water. Figures 7 to 16 displayed the thermal conductivities and thermal diffusivities for Al_2O_3 nanofluids as a function of particle size. Moreover, it displayed the dependence of the thermal conductivity and thermal diffusivity on the particle size, as well as, note that the slope increases as the particle size increase. The thermal conductivity and thermal diffusivity values of these nanofluids generally increase nonlinearly with increases particle size.

Table 1. Thermal conductivity and diffusivity of Al_2O_3 (nanofluids in distilled water)

Particles size (nm)	Volume fraction (%)	Thermal conductivity (W/m.K)	Thermal diffusivity (m^2/s)x10^{-7}	Enhancement in thermal conductivity (%)	Enhancement in thermal diffusivity (%)
11	1.40	0.676	1.7270	9.56	16.84
11	**1**.124	0.669	1.6738	8.42	13.24
11	0.845	0.661	1.6457	7.13	11.34
11	0.55	0.655	1.6219	6.32	9.73
11	0.225	0.646	1.5758	4.70	6.61
25	1.40	0.681	1.7344	10.37	17.34
25	**1**.124	0.674	1.6954	9.23	14.7
25	0.845	0.666	1.6549	7.94	11.96
25	0.55	0.658	1.6246	6.64	9.91
25	0.225	0.647	1.5790	4.86	6.83
50	1.4	0.689	1.7477	11.6	18.24
50	**1.**124	0.676	1.7050	9.56	15.35
50	0.845	0.668	1.6683	8.26	12.87
50	0.55	0.660	1.6272	6.96	10.09
50	0.225	0.648	1.5813	4.93	6.98
63	1.4	0.705	1.7930	14.26	21.31
63	**1.**124	0.695	1.7407	12.64	17.77
63	0.845	0.680	1.6880	10.21	14.2
63	0.55	0.669	1.6379	8.42	10.81
63	0.225	0.649	1.5836	5.18	7.1

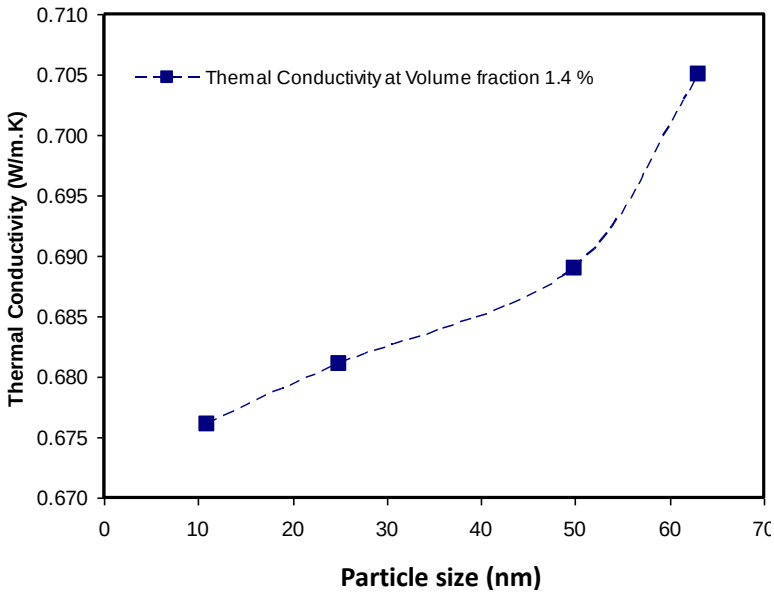

Figure 7. Variation of thermal conductivity of Al_2O_3 nanofluid with particle size obtained for 1.4 % volume fraction.

Furthermore, the thermal conductivity and thermal diffusivity of the smallest nanoparticles are lower than that of the largest nanoparticles. This would be attributed to phonon scattering at the solid–liquid interface. The

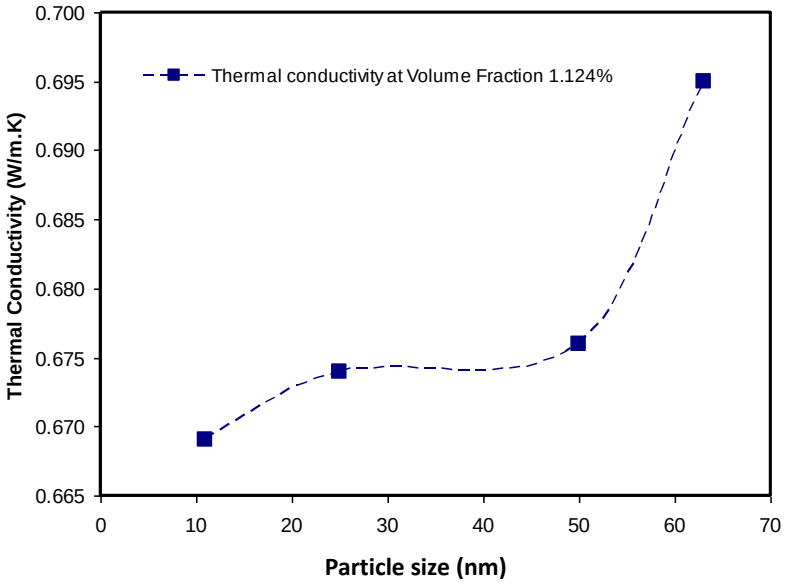

Figure 8. Variation of thermal conductivity of Al_2O_3 nanofluid with particle size obtained for 1.124 % volume fraction.

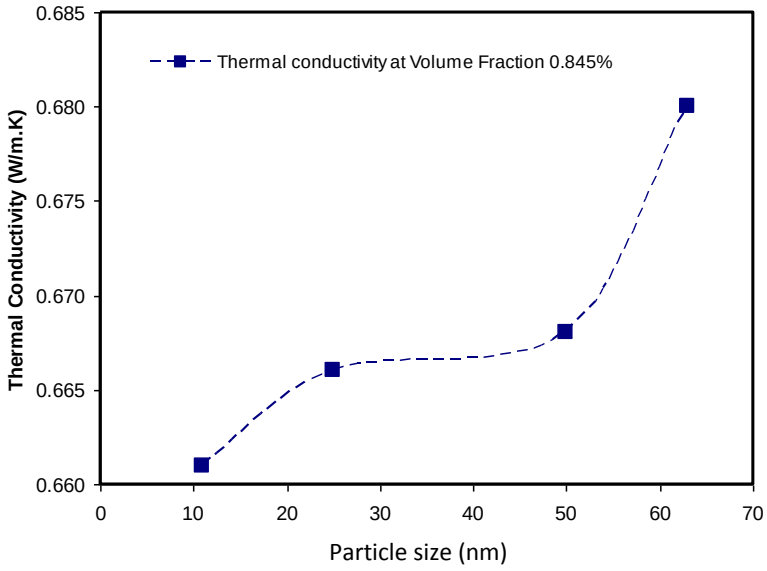

Figure 9. Variation of thermal conductivity of Al_2O_3 nanofluid with particle size obtained for 0.845% volume fraction.

phonon mean free path in small particles may be reduced by phonon–phonon scattering, scattering at the boundaries between nanoparticle and molecules, as well as, lattice imperfections. However, the relationship between the particle size and its thermal conductivity and thermal diffusivity are nonlinearly dependent for the particle size as shown in Figures 7 to 16.

The lattice imperfections in smaller nanoparticles cannot remarkably affect the thermal conductivity and thermal diffusivity. This indicates that, the phonon–phonon scattering at the boundary between nanoparticle and fluid interfacial can be more remarkable than that at the lattice imperfections. Though lattice imperfections are readily formed in small particles, the thermal conductivity and thermal diffusivity of nanoparticles is mainly subject to its size. Therefore, the results suggest that, the thermal conductivity of nanofluid is subject to a size-dependent effect. The results show that, the enhancement thermal

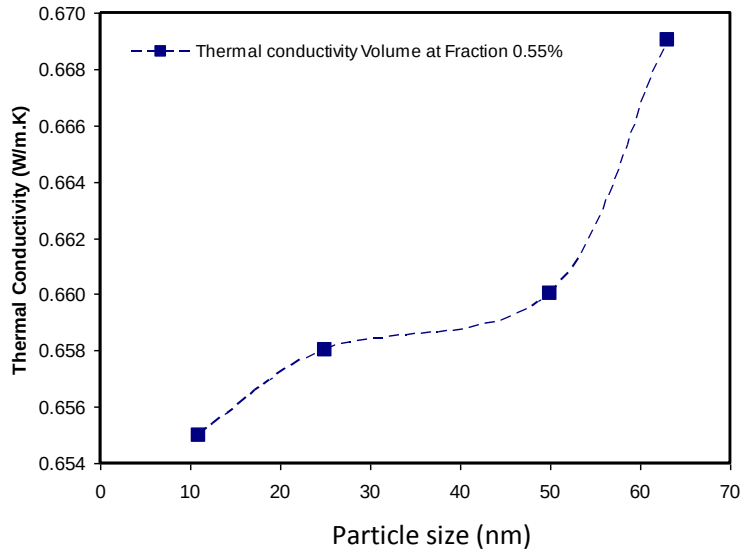

Figure 10. Variation of thermal conductivity of Al_2O_3 nanofluid with particle size obtained for 0.55 volume fraction.

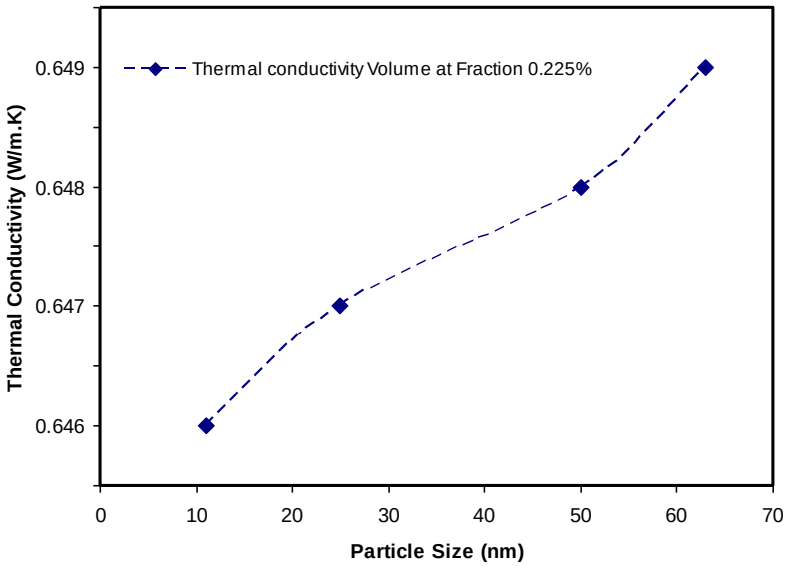

Figure 11. Variation of thermal conductivity of Al_2O_3 nanofluid with particle size obtained for 0.225% volume fraction.

conductivity were 9.56, 10.37, 11.6, 14.26% at particle size 11, 25, 50, and 63 nm at volume fraction 1.4%, respectively. While, the enhancement thermal diffusivity of Al_2O_3 nanofluid was 16.84, 17.34, 18.24, 21.31 at particle size 11, 25, 50, and 63 nm at volume fraction 1.4%, respectively. These results indicate that, the enhancement thermal conductivities and thermal diffusivities of Al_2O_3 nanoparticle suspension in distilled water have increased with increase in the particle size of nanoparticles. The results are listed in the Table 1.

Effect of volume fraction on thermal properties of nanofluids

Figures 17 to 24 shows the effect of volume fraction concentration on the thermal conductivity and thermal diffusivity of 11, 25, 50, 63 nm Al_2O_3 nanoparticles suspended in distilled water. The enhancement in thermal conductivity and thermal diffusivity increased with the increasing volume fraction concentration of nanoparticles. It is also observable that, the thermal

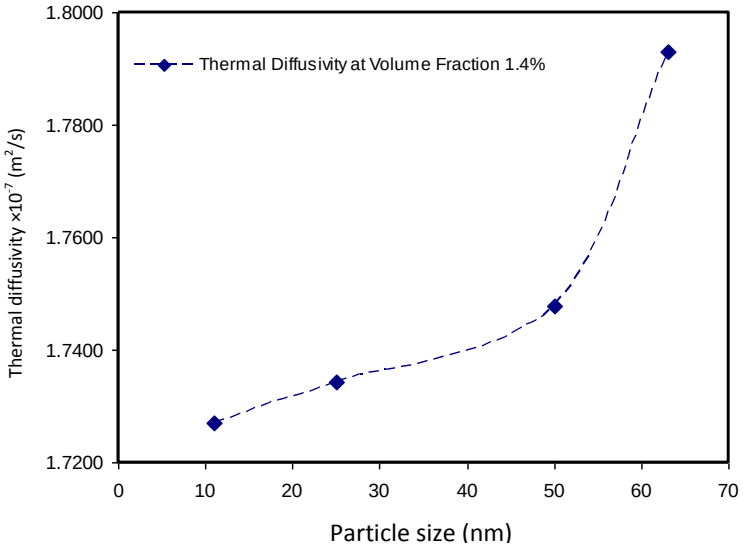

Figure 12. Variation of thermal diffusivity of Al_2O_3 nanofluid with particle size obtained for 1.4% volume fraction.

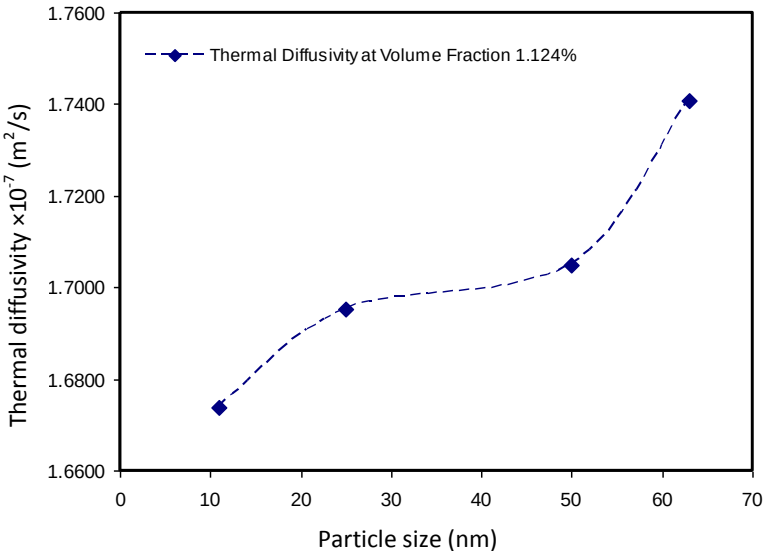

Figure 13. Variation of thermal diffusivity of Al_2O_3 nanofluid with particle size obtained for 1.124% volume fraction.

conductivity and thermal diffusivity increases linearly with the volume fraction concentration of nanoparticles. This observation can provide an insight into the mechanism of the thermal exchanger transport in nanofluids. We particularly mention the volume fraction concentration of nanoparticles dependence for thermal conductivity and thermal diffusivity in accordance with Figures 17 to 24, because the thermal conductivity and diffusivity would shows more enhancements if the nanoparticles formed suspensions in base fluids and this could be more profound in nanofluids containing a higher volume fraction of nanoparticles. Al_2O_3 (25 nm) nanofluid exhibit 10.37% enhancement with 1.4 % volume fraction of nanoparticles in distilled water while the nanofluid presents 9.23, 7.94, 6.64, 4.86% enhancement with 1.124, 0.845, 0.55, and 0.225 volume fraction nanoparticles in water, respectively. Al_2O_3 nanofluids exhibit 9.56, 8.42, 7.13, 6.32, and 4.70% enhancements with 1.4, 1.124, 0.845, 0.55, and 0.225% volume fraction concentration suspensions in distilled water, respectively. All results of Al_2O_3 of (11, 25, 50, and 63 nm) are listed in Table 1.

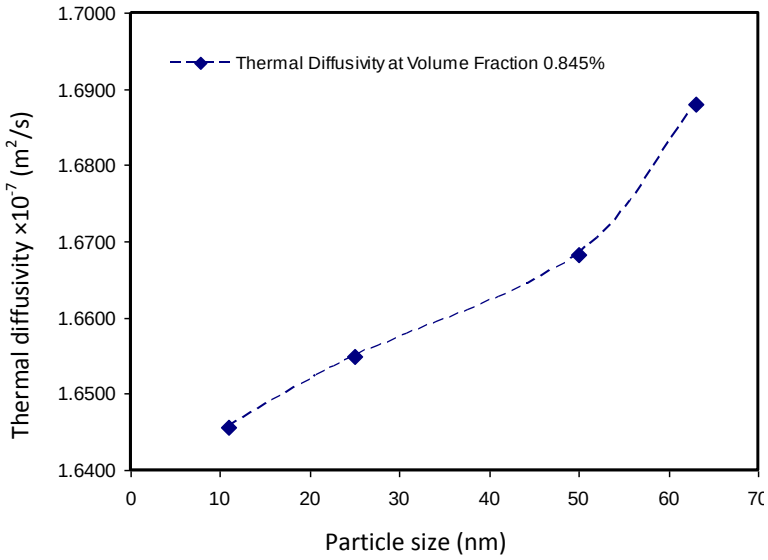

Figure 14. Variation of thermal diffusivity of Al_2O_3 nanofluid with particle size obtained for 0.845% volume fraction.

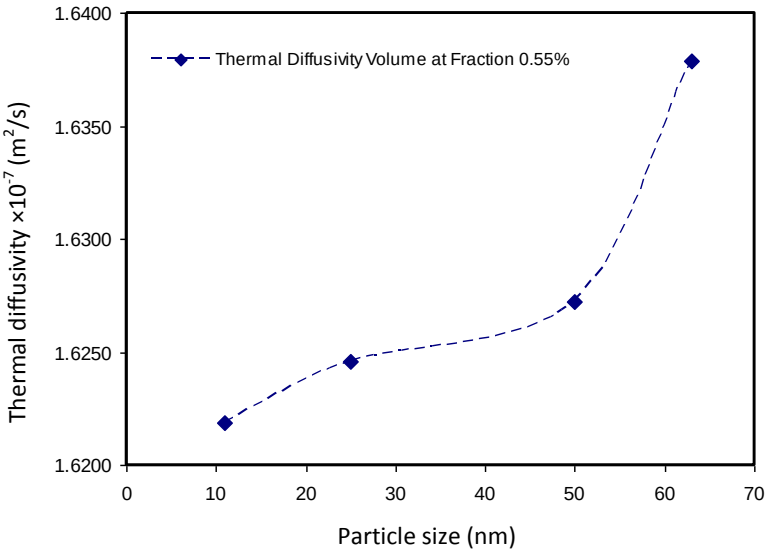

Figure 15. Variation of thermal diffusivity of Al_2O_3 nanofluid with particle size obtained for 0.55% volume fraction.

The nanoparticles suspension demonstrates some unique and novel thermal properties when compared to the traditional heat transfer of fluids. There are several mechanisms that will enhancement the thermal properties of nanofluids; Brownian motion of nanoparticles, interfacial layer between solid\fluids, nanoparticle structuring/aggregation, and effects of nanoparticle clustering (Liqiu, 2009). First, Brownian motion of nanoparticles could contribute to the thermal conduction enhancement through two ways, direct contribution due to motion of nanoparticles that transports heat, and indirect contribution due to micro-convection of fluid surrounding individual nanoparticles. The direct contribution of Brownian motion has been taken by comparing the time scale of particle motion with that of heat diffusion in the fluid. Equivalently, we can compare the time required for particle to move by the distance equal to its size with time required for heat to move in the liquid by the same distance (Liqiu, 2009; Keblinski et al., 2002). The indirect contribution has also been shown to

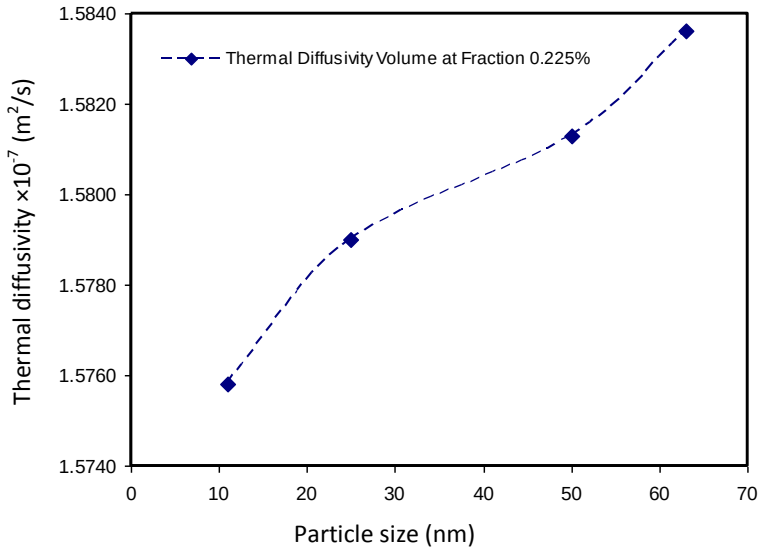

Figure 16. Variation of thermal diffusivity of Al_2O_3 nanofluid with particle size obtained for 0.225% volume fraction.

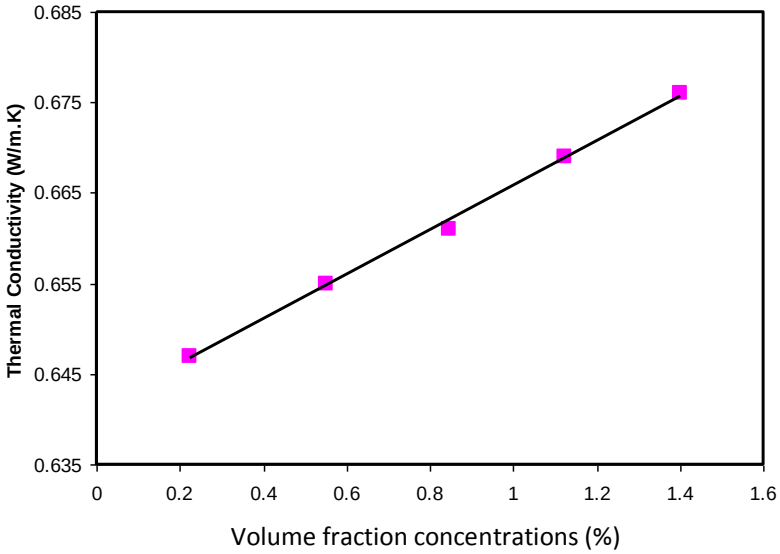

Figure 17. Thermal conductivity of Al_2O_3 (11nm) nanofluid as a function of Volume fraction concentration.

play a minute role through the same reasoning for the direct contribution and also through molecular modeling (Evans et al., 2006). Secondly, interfacial thermal resistance would lead to an increase in the estimate value of thermal conductivity of nanofluid and an increase thermal conductivity with increase particle size, which satisfy the experimental results.

An interface effect that could enhance thermal conductivity is the layering of the fluid at the solid interface, by which the atomic structure of the liquid layer is significantly more ordered than that of bulk liquid. Given that, crystalline solids (which are obviously ordered) display much better thermal transport than liquids, such liquid layering at the interface would be expected to lead to a higher thermal conductivity (Keblinski et al., 2002). To evaluate an upper limit for the effect of the interfacial layer, let us suppose that, the thermal conductivity of this interfacial fluid is exactly same as that of the solid nanoparticle. The resultant larger effective volume of the nanoparticle-layered-fluid

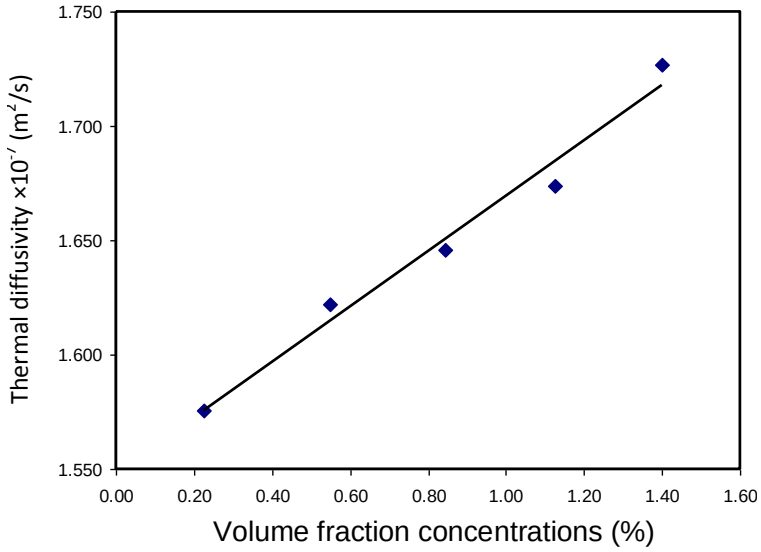

Figure 18. Thermal conductivity of Al_2O_3 (11nm) nanofluid as a function of volume fraction concentration.

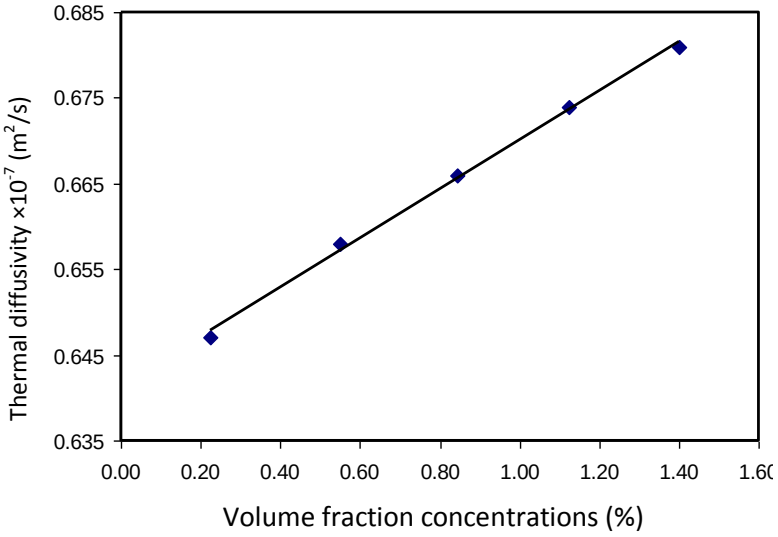

Figure 19. Thermal conductivity of Al_2O_3 (25 nm) nanofluid as a function of Volume fraction concentration.

structure could enhance the thermal conductivity of nanofluid. Third, nanoparticle structuring/aggregation have dominated mechanism for the thermal conductivity enhancement of nanofluids, due to interconnected nanoparticles in the fluid enhances the thermal conduction.

Lastly, by creating paths of lower thermal conductivity resistance, clustering of particles into percolating would have major effect on the effective thermal conductivity. The effective volume of cluster, that is, the volume from which other clusters are excluded, can be much larger than the physical volume of the particles. Since within such clusters, heat can move very rapidly, the volume fraction of highly conductive phase is larger than the volume of solid which is significantly increase thermal conductivity. The effect of clustering is depending on the ratio of the volume of the solid particles in the cluster to the total volume of the cluster. With decreasing packing fraction, the effective volume of the cluster increases, thus enhancing thermal conductivity. A further dramatic increase of enhancement thermal conductivity can take place if the nanoparticles do not need to be in physical

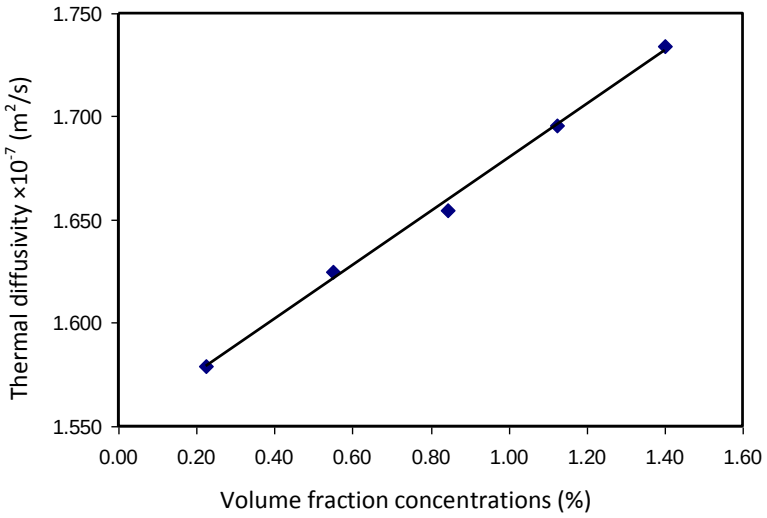

Figure 20. Thermal diffusivity of Al_2O_3 (25 nm) nanofluid as a function of Volume fraction concentration.

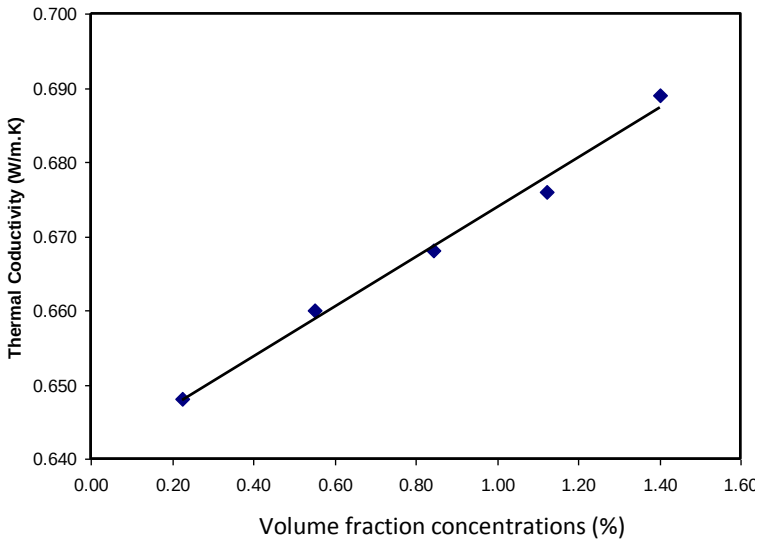

Figure 21. Thermal conductivity of Al_2O_3 (50 nm) nanofluid as a function of volume fraction concentration.

contact, but just within a specific distance, allowing rapid heat flow between them. Such fluid-mediated clusters exhibit a very low packing fraction and thus, a very large effective volume. The principal is capable of explaining the unusually large experimental observed in enhancement of the thermal conductivity (Keblinski et al., 2002).

The results shows significant enhancement in the thermal conductivity and thermal diffusivity of Al_2O_3 nanofluid. For example, the nanofluid with the particle size of 11 nm, the enhancement of thermal conductivity and thermal diffusivity were recorded and it varies from 4.70 at 0.225% volume fraction to 9.56 at 1.4%, and 6.61 at 0.225% volume fraction to 16.84 at 1.4% volume fraction respectively. However, for nanofluid with the particle size 63 nm, the thermal conductivity varies from 5.18 at 0.225% volume fraction to 14.26 at 1.4% volume fraction. While, thermal diffusivity varies from 7.1 at 0.225% to 21.31 at 1.4% volume fraction.

Conclusion

The coupled transient heat conduction equations of the

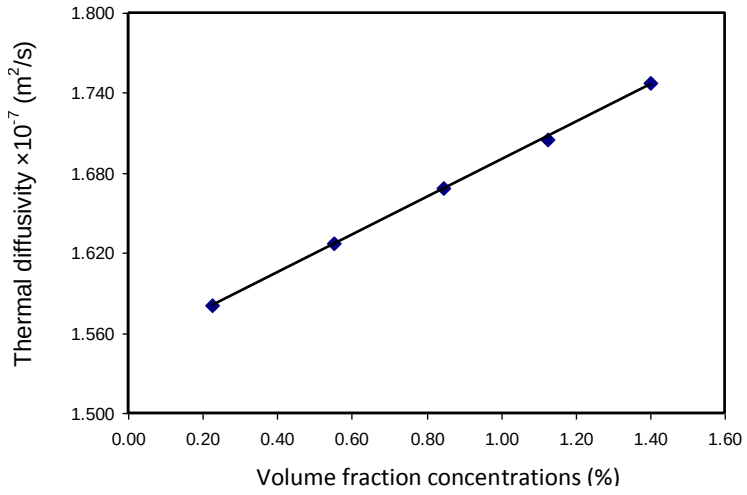

Figure 22. Thermal diffusivity of Al_2O_3 (50 nm) nanofluid as a function of volume fraction concentration.

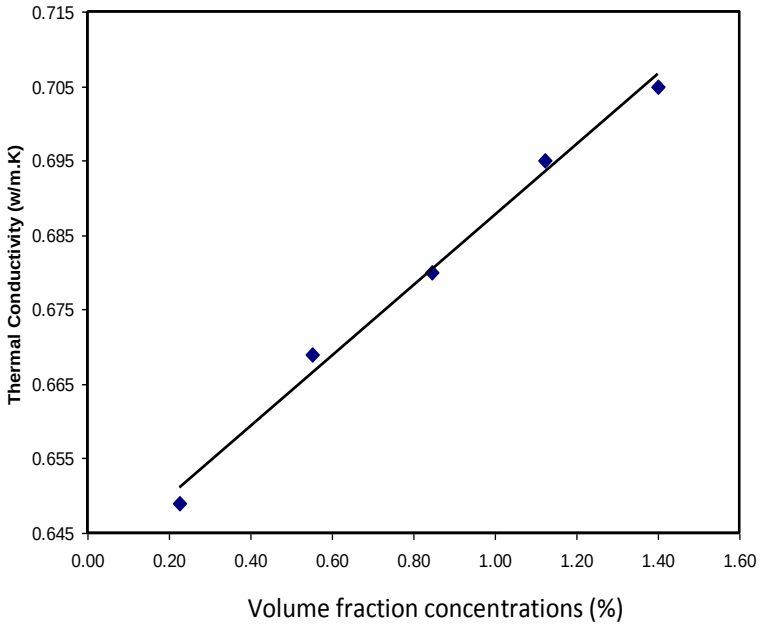

Figure 23. Thermal conductivity of Al_2O_3 (63 nm) nanofluid as a function of volume fraction concentration.

heating wire and the nanofluid were solved simultaneously using the finite difference Method based on Crank- Nicolson algorithm to get thermal conductivity and thermal diffusivity of Al_2O_3 (11, 25, 50, and 63 nm) nanofluids. Crank-Nicolson algorithm was used to discretize the coupled transient heat conduction equations. New experimental data of the thermal conductivity and thermal diffusivity of Al_2O_3 (11, 25, 50, and 63 nm) nanoparticles suspension in distilled water were obtained in this study.

Results show that, the thermal conductivity and thermal diffusivity are increase with increasing the particle size and volume fraction concentration. Since our measurements were carried at room temperature the Brownian motion effect can be ignored, thus, our results show that, interfacial layer between solid/fluids, nanoparticle structuring/aggregation particle clustering, particle size, and the volume fraction concentration of particles in the water base fluid give a significant effect on thermal conductivity and thermal diffusivity of nanofluids.

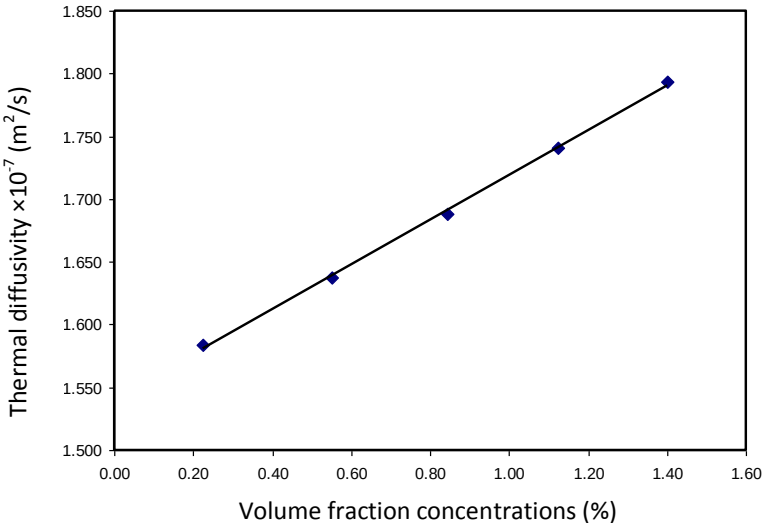

Figure 24. Thermal diffusivity of Al_2O_3 (63 nm) nanofluid as a function of volume fraction concentration.

ACKNOWLEDGEMENTS

We gratefully acknowledge the Department of Physics, UPM for providing the research facilities to enable us to carry out this research. We also like to acknowledge Ministry of Education for the financial support through Fundamental research grant (01-11-08-664FR/5523664) and University research grant (05-02-12-2179RU).

REFERENCES

Calvin HL, Peterson GP (2007). The Effect of Particle Size on the Effective Thermal Conductivity of Al2O3-Water Nanofluids. J. Appl. Phys. 101(4):044312-044316.

Calvin HL, Peterson GP (2010). Experimental Studies of Natural Convection Heat Transfer of Al_2O_3/DIWater Nanoparticle Suspensions (Nanofluids). Adv. Mech. Eng. pp. 1-10.

Choi SUS (1998). Nanofluid technology: Current Status and Future research, Korea-US Technical Conf. on Strategic Technologies, Vienna, V.A.

Choi SUS, Zhang Z, Yu W, Lockwood FE, Grulke EA (2001). Anomalous Thermal Conductivity Enhancement in Nanotube Suspensions. Appl. Phys. Lett. 79:2252-2254.

Eastman J, Choi SUS, Li S, Thompson LJ, Lee S (1997). Enhanced Thermal Conductivity Through The Development of Nanofluids. Mater. Res. Soc. Symptoms. 457:3-11.

Evans W, Fish J, Keblinski P (2006). Role of Brownian motion Hydrodynamics on Nanofluids Thermal Conductivity. Appl. Phys. Lett. 88(9):093116-093118.

Jonathan DS, Richard ER, Robert JS (1990). Collinear Photothermal Deflection Spectroscopy With Light Scattering Samples. Appl. Optics. 29(28):4225-4234.

Keblinski P, Phillpot SR, Choi SUS, Eastman JA (2002). Mechanisms Of Heat Flow in Suspensions of Nano-Sized. Int. J. Heat Mass Transfer. 45:855-863.

Kim SH, Choi SR, Kim D (2007). Thermal Conductivity of Metal-Oxide Nanofluids: Particle Size Dependence and Effect of Laser Irradiation. J. Heat Transfer. 129:298-307.

Lee S, Choi SUS, Li S, Eastman J (1999). Measuring thermal conductivity of fluids containing oxide nanoparticles. J. Heat Transfer ASME. 121(2):280-289.

Liqiu W (2009). Advances in Transport Phenomena, Springer-Verlag Berlin Heidelberg.

Maiga S, Nguyen C, Galanis N, Gilles R, Thierry M, Mickael C (2006). Heat Transfer Enhancement in Turbulent Tube Flow Using Al_2O_3 Nanoparticle Suspension. Int. J. Numer. Methods Heat Fluid Flow. 16:275-292.

Michael PB, Yanhui Y, Pramod W, Amyn ST (2009a). The Thermal Conductivity of Alumina Nanofluids in Water, Ethylene Glycol, and Ethylene Glycol + Water Mixtures. J. Nanopart. Res. 12(4):1469-1477.

Michael PB, Yanhui Y, Pramod W, Amyn ST (2009b). The Effect of Particle Size on the Thermal Conductivity of Alumina Nanofluids. J. Nanopart. Res. 11:1129-1136.

Omid A, Ahmad F (2009). Numerical Investigation of Natural Convection of Al_2O_3 Nanofluid in Vertical Annuli. Heat Mass Transfer. 46(1):15-23.

Pang C, Kang YT (2012). Stability and Thermal Conductivity Characteristics of Nanofluids (H_2O/CH_3OH + NaCl + Al_2O_3 Nanoparticles) for CO_2 Absorption Application. International Refrigeration and Air Conditioning Conference at Purdue.

Walvekar R, Faris IA, Khalid M (2012). Thermal Conductivity of Carbon Nanotube Nanofluid – Experimental and Theoretical Study. Heat Transfer – Asian Res. 41:145-163.

Wang X, Xu X, Choi SUS (1999). Thermal Conductivity of Nanoparticle-Fluid Mixture. J. Thermophy. Heat Transfer. 13:474-480.

Wen D, Ding Y (2006). Natural Convective Heat Transfer of Suspensions of Titanium Dioxide Nanoparticles (Nanofluids). IEEE Trans. Nanotechnol. 5(3):220-227.

Wen QL, Qing MF (2008). Study for the Particle's Scale Effect on Some Thermophysical Properties of Nanofluids by a Simplified Molecular Dynamics Method. Eng. Anal. Bound. Elem. 32:282-289.

Wongwises S, Weerapun D (2007). A Critical Review of Convective Heat Transfer of Nanofluids, Renew. Sustain. Energy Rev. 11:797-817.

Yimin X, Wilfried R (2000). Conceptions for Heat Transfer Correlation of Nanofluids, Int. J. Heat Mass Transfer. 43:3701-3707.

academicJournals

Vol. 8(28), pp. 1458-1463, 30 July, 2013
DOI: 10.5897/IJPS12.368
ISSN 1992 - 1950 © 2013 Academic Journals
http://www.academicjournals.org/IJPS

International Journal of Physical Sciences

Full Length Research Paper

Modelling of solar radiation for West Africa: The Nigerian option

Cecily Nwokocha[1], Raymond Kasei[2] and Urias Goll[3]

[1]Department of Physics, Alvan Ikoku Federal College of Education, P. M. B. 1033 Owerri, Imo State, Nigeria.
[2]Centre for Development Research, University of Bonn, Germany.
[3]Department of Environmental Studies, University of Liberia, Liberia.

Accepted 29 July, 2013

The United Nations Framework Convention on Climate Change (UNFCCC) reports indicate that those who are least responsible for climate change are also the most vulnerable to its projected impacts. In no place is this more evident than in Sub Saharan Africa, where greenhouse gas (GHG) emissions are negligible from a global scale. In Africa, energy demands could be the major factor that may lead to the increase of its emissions in the very near future. Forests are being used up for domestic energy supply. Oil produced energy increases carbon foot prints and hydropower is unreliable due to uncertainties in rainfall patterns. By 2004, the energy consumption mix of West Africa was dominated by oil (58%), followed by natural gas (38%) and hydroelectric (8%) with coal and other energy forms not part of the mix. The Sayigh's universal equation is presented in this work, for estimating the global solar radiation analysing data from 1972 to 2004 in Nigeria using Umudike, as a case study. The global solar radiation within the region was noted to range from 1.99 to 6.75 kWh indicating that the method could be used in producing signatures of global solar radiation in Nigeria when actual measurements are not available.

Key words: Solar radiation, modelling, West Africa, Nigeria.

INTRODUCTION

Countries in West Africa face many of the same challenges as the rest of the world due to growing fuelling energy demand. Besides few exceptions such as Nigeria, the countries in the region do not have or have developed sufficient domestic resources so they have become dependent on imports. State companies which dominate the energy sector lack commercial incentives and tend to be inefficient; prices of fuels such as kerosene, diesel and electricity are heavily subsidized encouraging inefficient use of energy, deterring additional investment in energy supply and often resulting in shortages and rationing (Taimur et al., 2007).

Notwithstanding, combustion of these fuels for power supply unleashes intolerable amounts of carbon (iv) oxide as well as other harmful gases to the environment thus contributing in turning the earth's atmosphere to a greenhouse with the harmful effect of producing global warming. The environmental implications of gas emission from these sources including gas flaring are part of issues that informed the Copenhagen Climate Change Summit at Denmark in December 2009. The summit was aimed at creating global awareness of climate change as well as establishing treaties that can be supported by global businesses.

*Corresponding author. E-mail: doncecily@yahoo.com. Tel: +234 8037075060.

This paper aims at recommending West Africa and Nigeria in particular to renewable energy, having estimated levels of global solar radiation at Umudike (latitude 5.29°N, longitude 7.33°E) Eastern Nigeria, using the Angstrom universal method from the period 1972 to 2004. Already, many countries like the United States of America, China, India and Brazil etc, are employing this initiative by the United Nations to start-up the clean development mechanism project, such as the use of solar power generation; biofuel generation from waste and investment in carbon trading amongst other things, geared at making the environment free from harmful emissions. With advancement in science and technology, the initiation to use solar energy for power generation is already in use towards meeting electricity needs. There are indications that the desire to diversify sources of electricity generation may become visible, following plans by the country's first solar electricity generation company to commence operation before the end of the year (Chineke, 2002; Igbal, 1983). The purpose of the work is to use different models for estimating global solar radiations in Nigeria for locations where no measured data is available.

MATERIALS AND METHODS

Study area

Nigeria is located in the tropics between 3°E to 14°E of longitude and 4°N to 14°N of latitude. She is endowed with an annual average daily sunshine of 6.25 h ranging between 3.5 h at the coastal areas and 9.0 h at the far northern boundary. The minimum and maximum hours of sunshine amount to 0.1 and 9.9 h respectively. Similarly, it has an annual average daily solar radiation of about 5.25 kWh/m^2 per day varying between 3.5 kWh/m^2 per day at the coastal areas and 7.0 kWh/m^2 per day at the Northern boundary. The minimum and maximum temperatures are 9.7 and 41.5°C respectively (Akinbami, 2001).

Acquisition of data

A monthly average temperature data obtained from the National Root Crop Research Institute (NRCRI) Umudike, for the period of 30 years ranging from 1972 to 2004 was used for this research work. The three models of estimating solar radiation is presented in this work but only the Sayigh's method was used to plot the signatures because of its accuracy, hence the three models were compared by combining all the models. In spite of the importance of global solar radiation data, few meteorological stations, especially in developing countries such as Nigeria measure these data accurately and continuously. The situation can be solved using equation methods that estimate global solar radiation from available meteorological parameters such as sunshine duration, daily temperature, relative humidity e.t.c (Akpabio and Etuk, 2003; Akpabio et al., 2005; Chineke, 2008). The correlation model developed can be used in estimating global solar radiation in locations of similar latitude, altitude and climatology. Empirical modelling is an essential and economical tool for the estimation of global solar radiation. There are several methods available for estimating global solar radiation (Chiemeka and Chineke, 2009; Chineke, 2008); however, for this work the following were considered.

Sayigh's equation

Sayigh proposed his universal formula for the estimation of total radiation intensity (Sayigh, 1977; El-Sahaam and Sayigh, 1979; Oduro-Afriyie, 1997), which relates the global solar radiation Rg, to mean maximum temperature Tmax, mean relative humidity RH, and the ratio of sunshine hours to the length of the day S1, expressed as:

$$Rg = NK \exp\{\varphi(S1 - RH/15 - 1/Tmax)\} \quad (1)$$

Where

$$N = 1.7 - 0.458\varphi \quad (2)$$

and

$$K = 1.163\ (a\ Z + bij\ Cos\ \varphi) \quad (3)$$

is a constant ($^{KWh/m^2/day}$)

$$a = 0.2/(1 + 0.1\varphi - - - - - - \quad (4)$$

φ, the latitude in degrees; Z is the length of day in hours; the monthly average is taken in the middle of the month; K, N and a, are factors which can be computed using the equation above. bi j is a humidity factor, i=1,2,3 where 1 is for RH < 65%, 2 is for RH > 70%, and 3 is for 65% $\leq$ RH $\leq$ 70%. On the other hand, j = 1, 2, 3… 12 which refers to the months of the year.

Hargreave's equation

Chineke and Jagtap (1995) compared 3 models and got the best fit with the modified temperature based Hargreave's method (Hargreaves and Samani, 1982). The temperature-based model is most appropriate when data on sunshine hours is lacking like in the case for Nigeria. Chineke et al. (1999) proposed the equation for estimating solar radiation and presented it in the form:

$$Rs = 0.16RaTd_{1/2} \quad (5)$$

Where R_S = solar radiation, T_d = daily temperature difference (maximum minus minimum) values, Ra = extraterrestrial solar radiation (generated by a computer routine and requiring the locations grid parameter).

Angstrom equation:

This is one of the most popular models. It is a regression equation (Angstrom, 1924; 1929 and Black et al., 1954), which relates global solar radiation H, to the duration of sunshine S, being the parameter mostly readily measured at meteorological stations.
The model is thus expressed:

$$H + Ho = a + bs/Z \quad (6)$$

H = total horizontal solar radiation
Ho = extraterrestrial solar radiation

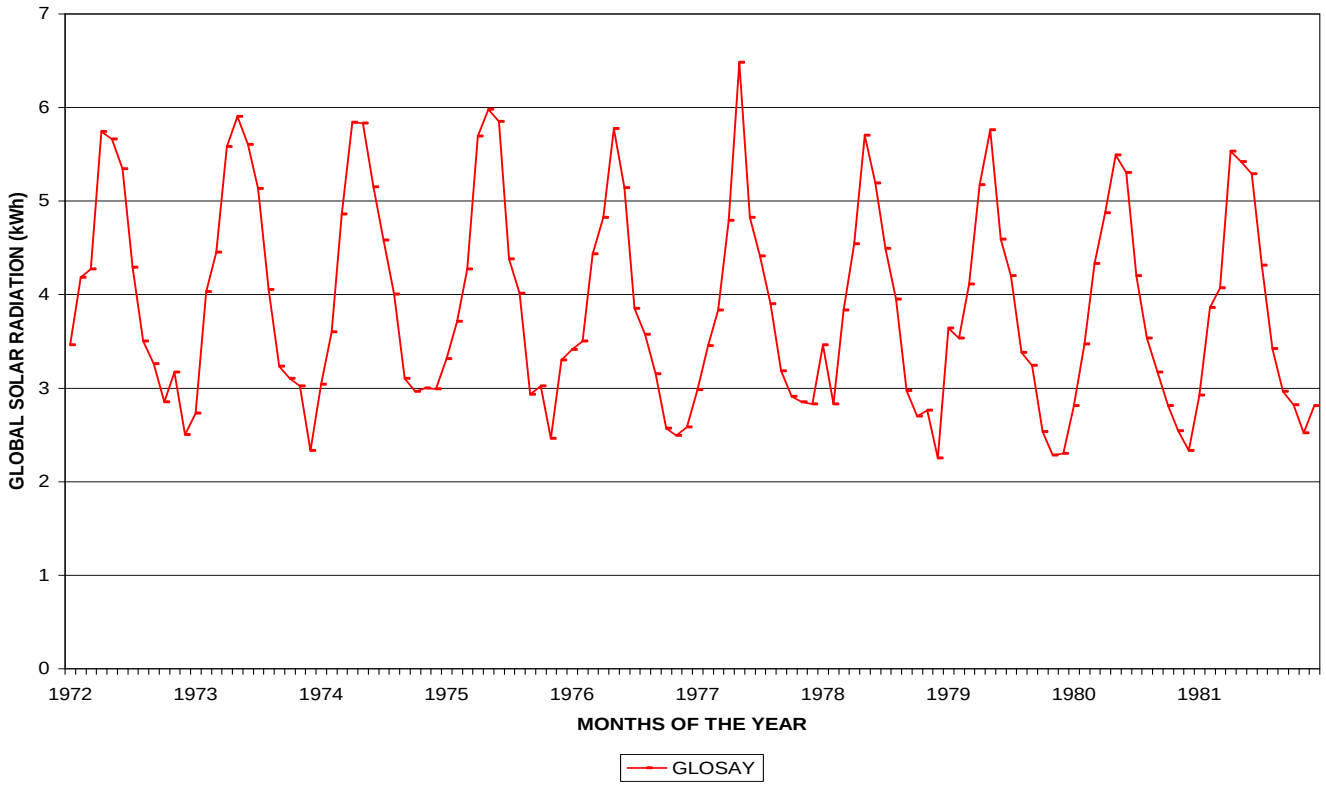

Figure 1. Global Solar Radiation for the first decade between 1972 to 1981.

S = Average sunshine hours per month
Z = length of the day in hours, the monthly average is taken in the middle of the month a and b are constants.

From the daily averages of the temperature and sunshine hour data, the global solar radiation was estimated for the region (Angstrom, 1924, 1929; Oduro-Afriyie, 1997; Chineke et al., 1999; Hargreaves and Samani, 1982; Taimur et al., 2007; Chineke, 2008; Chiemeka and Chineke, 2009). This would highlight how much the clearness index for the region could be established (Akpabio et al., 2005; Babatunde and Aro, 1995). For this analysis, the period of the study was grouped into four decades, ranging from 1972 to1981 for the first decade, 1982 to 1991 for the second decade, 1992 to 2001 for the third decade and the forth decade being the years from 2002 to 2004.

RESULT AND DISCUSSION

In Figures 1 to 3, the signatures of the estimates were shown creating a trend line for modelling and subsequently, the expected levels of solar radiation within the region. Within the first decade, the region recorded a maximum of 6.48 kWh in 1977 and a minimum of 2.25 kWh in 1978. However, the records of the estimated maximum levels of solar radiation that reached the region for the decade were 5.74 kWh in 1972; 5.9 kWh in 1973; 5.84 kWh in 1974; 5.98 kWh in 1975; 5.77 kWhin 1976; 5.7 kWh in 1978; 5.76 kWh in 1979; 5.49 kWh in 1980 and 5.53 kWh in 1981; as shown in Figure 1. From Figure 2, the trend line of the estimates of the second decade was similar to the first although with variation in the estimated maximum solar radiation, which was 6.23 kWh in 1988 and a minimum of 1.99 kWh in 1985. However, the records yet reflect the potentials of harnessing this source of renewable energy in areas of photovoltaic in rural electrification (Chineke, 2008; Chineke et al., 2007), evapotranspiration and agronomy (Okoro et al., 2008), to mention but a few.

The third decade ranging from 1992 to 2001 had its signature similar to those previously discussed. From Figure 3, the estimate showed the highest level in the maximum solar radiation within the period of study, which was 6.75 kWh in 1998, with similar high records of 6.06; 5.87; 6.05 and 5.98 kWh in the years 1995; 1996; 1997 and 2001 respectively. This could not be far from the truth as this period recorded the highest awareness on global warming and climate change. The gaps in the data were mainly due to unavailability of measurements of the variables for the months within the period.

Figure 4 showed that the levels of solar radiation were also high with maximums of 5.92, 6.09 and 6.1 kWh in the years 2002, 2003 and 2004 respectively; having minimums of 2.58, 2.38 and 2.5 kWh in the years 2002, 2003 and 2004 respectively. These earlier figures

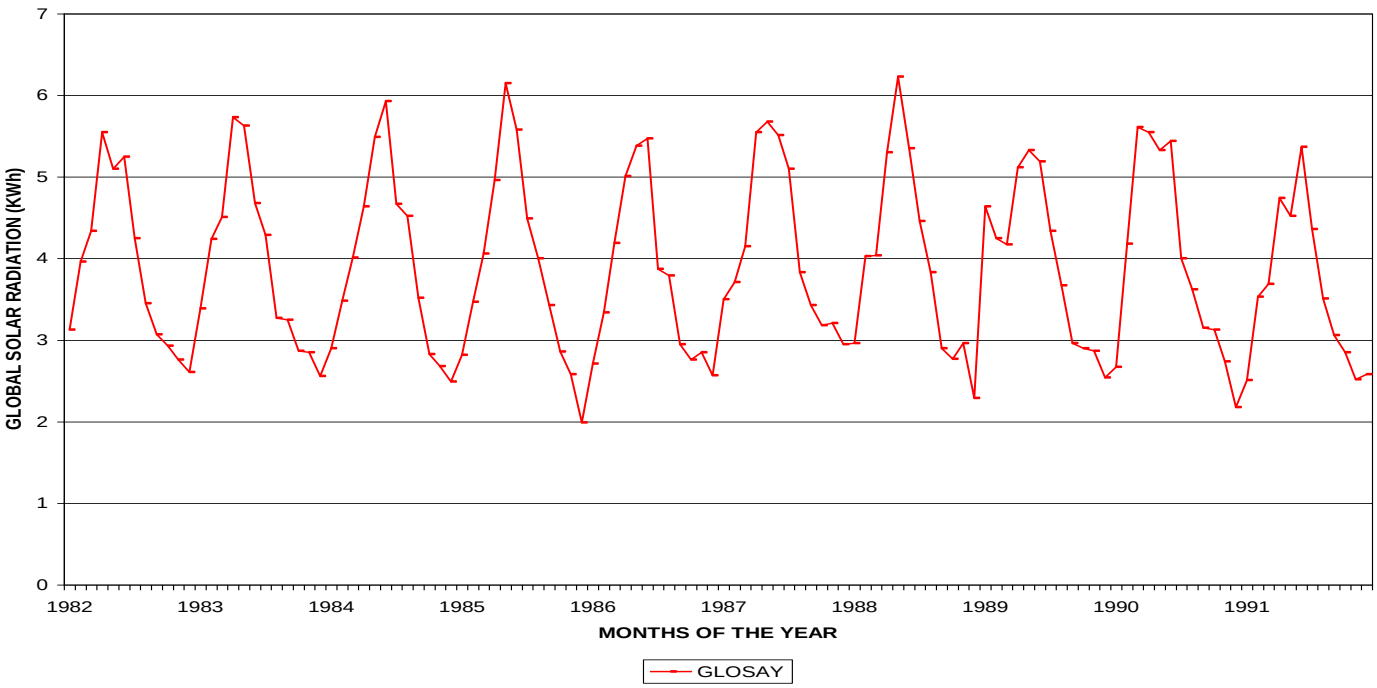

Figure 2. Global solar radiation for the second decade between 1982 to 1991.

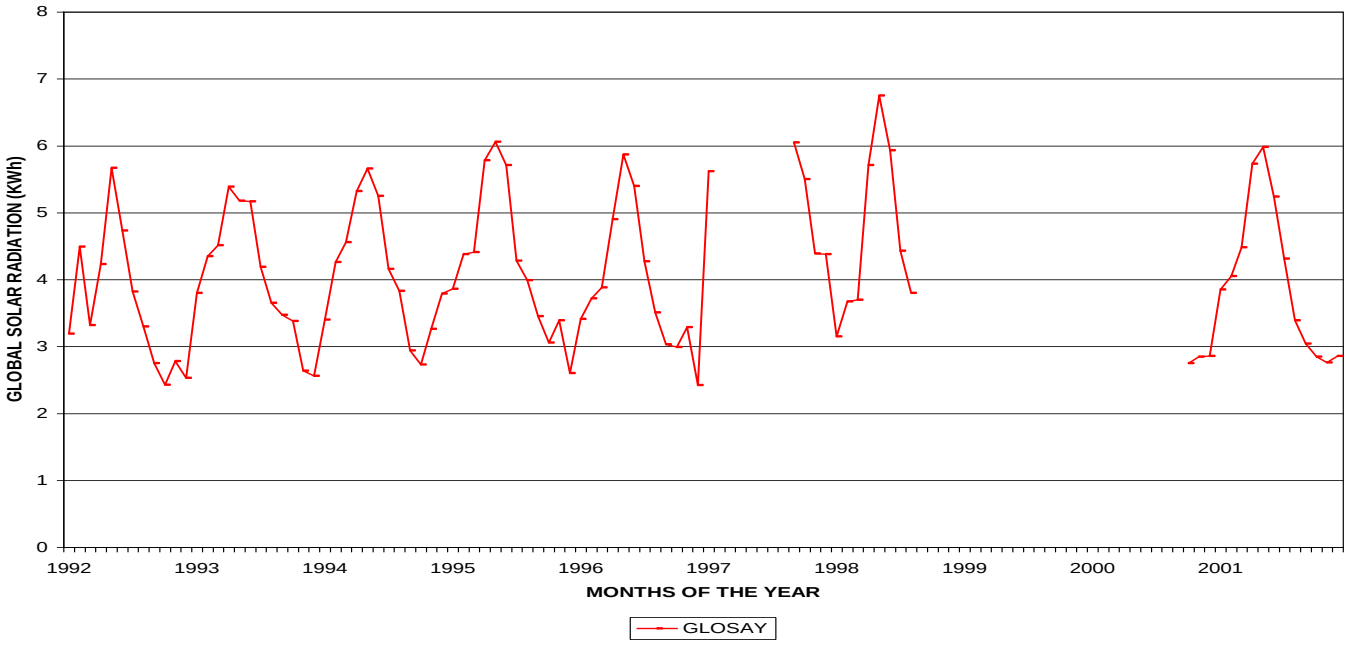

Figure 3. Global solar radiation for the third decade between 1992 to 2001.

revealed that the power need of Nigeria, most especially those within the South-eastern region, could be addressed if the potentials of this renewable energy is adequately harnessed. However, comparing the results from the Sayigh universal formula with those obtained using Angstrom and Hargreaves estimation methods yet over the region as shown in Figure 5; it could be seen that the trend line was similar hence showing an

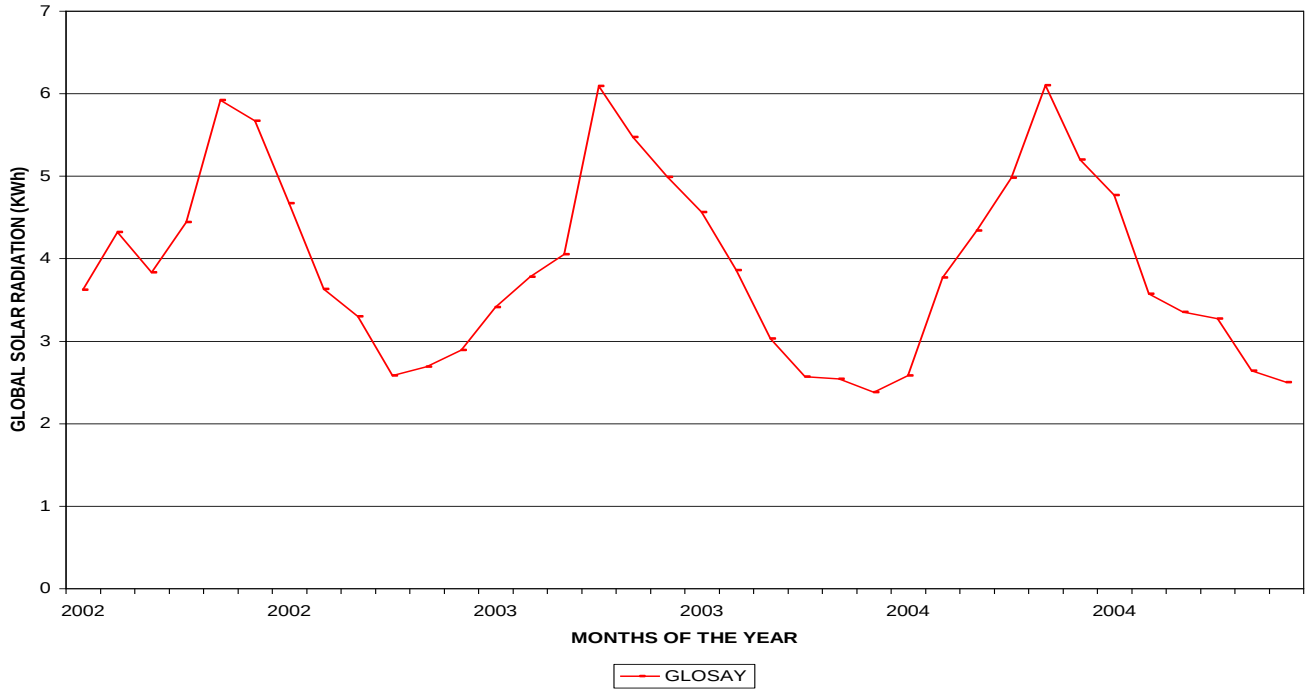

Figure 4. Global solar radiation for the last three years in the fourth decade between 2002 to 2004.

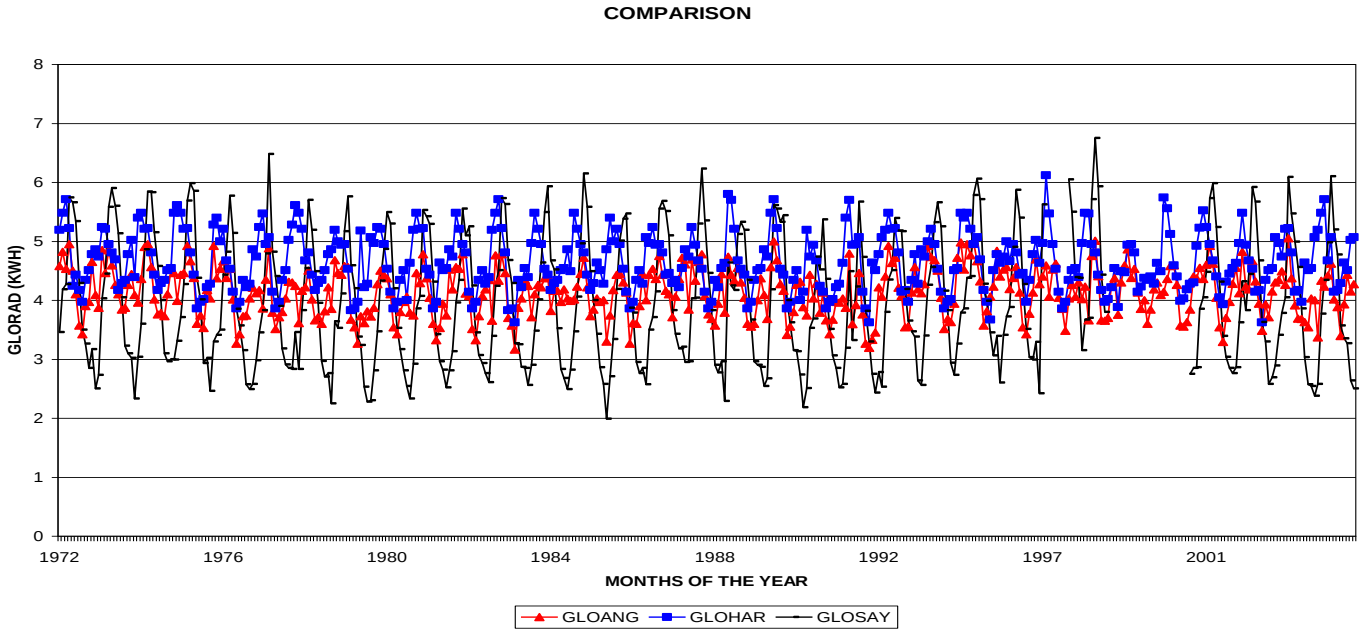

Figure 5. Comparison of levels of Global Solar Radiation at Umudike with the three estimation methods from 1972-2004.

agreement within each estimation method.

Conclusion

From the analyses, it is seen that the levels of global solar radiation recorded over the region were high having least values over the harmattan months as also reported in Chineke et al. (2007). These values are adequate in citing Photovoltaic systems (PV) as there is enough energy to power them all year round (Chiemeka and

Chineke, 2009). Designing and constructing solar cookers, incubators, ovens and preserving equipments that would be affordable but efficient for those living in the rural areas within the study area, becomes necessary as majority of the people living in these area are poor. This will in turn, enhance their living standard (Chineke and Igwiro, 2008), which is one of the objectives of the Millennium Developmental Goals (MDG) of the government.

Photovoltaic systems are now the lowest cost option for satisfying many of the electrical energy needs of areas not served by distributed electricity, particularly in developing countries, located in the tropics, where the amount of sunshine is generally high and rural household electricity consumption is comparatively low. Efforts should therefore be made to improve the number of meteorological stations available so that observations may be obtained from these stations to cover a wider scope.

REFERENCES

Akinbami JFK (2001). Renewable Energy Resources and Technologies in Nigeria: Present Situation, Future Prospects and Policy Framework. Mitigation and Adaptation Strategies for Global Change. 6:155-188. Kluwer Academic Publishers. Netherlands.

Akpabio LE, Etuk SE (2003). Relationship Between Global Solar Radiation And Sunshine Duration For Onne, Nigeria. Turk J. Physics, 27:161-167.

Akpabio LE, Udo SO, Etuk SE (2005). Modeling Global Solar Radiation For A Tropical Location: Onne, Nigeria. Turk J. Physics, 29:63-68.

Angstrom A (1924). Solar and terrestrial radiation. Q. J. R. Meteorol. Soc. 50:121-125.

Angstrom A (1929). Recording Solar Radiation. Medd. Statues meterol. Hyd. Anstalt. 3:4-10.

Black JR, Bonython CW, Precott J (1954). Solar Radiation And The Duration Of Sunshine. Quart J. Roy. METEOR. 80:231-235.

Babatunde EB, Aro TO (1995). Relationship Between "Clearness Index" And "Cloudiness Index" At A Tropical Station (Ilorin, Nigeria), Renewable Energy, 6(7):801-805.

Chiemeka IU, Chineke TC (2009). Evaluating the global solar energy potential at Uturu, Nigeria. Int. J. Phys. Sci. 4(3):115-119. Available Online at http://www.academic journals.org/IJPS.

Chineke TC (2002). A Robust Method Of Evaluating The Solar Energy Potential Of A Data Sparse Site, The Physical Scientist, 1:59-69.

Chineke TC (2008). Equations for estimating global solar radiation in data sparse regions. Renewable Energy 33(4):827-831.

Chineke TC, Aina JI, Jagtap SS (1999). Solar Radiation Database for Nigeria, Discovery & Innovation, 11(3/4):207-210.

Chineke TC, Igwiro EC (2008). Urban and rural electrification: enhancing the energy sector in Nigeria using photovoltaic technology, UNESCO/ANSTI Afr. J. Sci. Technol. 9(1):102-108.

Chineke TC,Jagtap SS (1995). A Comparison of Three Empirical Models For Estimating Solar Radiation In Nigeria. Afr. J. Sci. Technol. Series A, 11:45-48.

Chineke TC, Okoro UK, Igwiro CE (2007). The Imperatives Of Solar Photovoltaic As Viable Options for Rural Electrification in Nigeria. Int. J. Nat. Appl. Sci. 3(2):193-199.

El-Sahaam MA, Sayigh AA M (1979). Estimation of Diffuse Solar Radiation In The Arabian Pem Proc. Symp. On Radiation in The Atmosphere. Ed. J. A. Book Sc. Press, pp. 607-610.

Hargreaves GH, Samani ZA (1982). Estimating Potential Evapotranspiration. J. Irrig. Drainage Engr. 108(IR3):225-230.

Igbal M (1983). An introduction to solar radiation. Academic Press, New York.

Oduro- Afriyie K (1997). Performance of Sayigh's universal formula for the estimation of global solar radiation in Ghana. Renewable Energy, 10(1):91-106.

Okoro UK, Chineke TC, Nwofor Ok, Ibe A (2008). Evapotranspiration Levels At Owerri In The Niger Delta Nigeria. Int. J. Nat. Appl. Sci. 4(2):168-173.

Sayigh AAM (1977). Estimation of total radiation intensity a universal formula in 4th course of solar energy convention, Vol. II Mancin and Quercia I. F. (Eds), ICTP, Trieste, Italy.

Taimur B, Amine M, David C, Joseph N (2007). IMF Working Paper No. 07/71, March 2007.

academicJournals

Vol. 8(28), pp. 1464-1469, 30 July, 2013
DOI: 10.5897/IJPS07.031
ISSN 1992 - 1950 © 2013 Academic Journals
http://www.academicjournals.org/IJPS

International Journal of Physical Sciences

Full Length Research Paper

Novel method of iron removal from underground dug well waters in communities around Okada town, Ovia North-East L.G.A. Edo State

Chike Luke Orjiekwe*, Kehinde Oguniran and Solola Saheed Abiodun

Department of Chemical Sciences, Igbinedion University, Okada, Edo State Nigeria.

Accepted 29 July, 2013

Some indices of pollution were studied in water samples from 25 dug wells randomly selected from Okada town and it's environ. Physicochemical parameters measured include temperature, pH, colour, turbidity, total dissolved solids (TDS), toxic shock syndrome (TSS), total hardness, Ca, Mg, Fe, Mn, nitrate and phosphate etc. The results of the study showed that dug wells from this area contain Fe and Mn concentrations in nuisance quantity, far in excess of WHO recommended limits, with obvious consequence for drinking and domestic uses. The use of sodium hydroperoxide, a powerful oxidant for the removal of the Fe and Mn from the dug well water samples is described. This novel method is preferable to most conventional methods because it is cost effective, environmentally friendly, very fast and easy to apply.

Key words: Iron removal, dug well water, sodium hydroperoxide.

INTRODUCTION

Ground water in form of springs, dug wells or borehole are major sources of drinking and domestic water usage throughout the world (Masters, 1998; Sharmer et al., 2005). It is considered better than surface water because it is free from pollutants and other harmful pathogens (Sharmer et al., 2005). However, in some locations, ground water contains dissolved ions such as ferric and ferrous ions, either from geological formation or from iron pump components.

Iron can be present in water either as ferrous iron, ferric iron, organic iron or iron bacteria (Machmeier, 1971). Based on taste and nuisance considerations, the World Health Organization (WHO) recommends that the iron concentration in drinking water should be less than 0.3mg/l (WHO, 1996). Iron concentration in excess of 0.3mg/l is undesirable in drinking water as it causes several aesthetic and operational problems including bad taste, discolouration, staining and deposition in distribution systems (Sharmer et al., 2005).

Several methods namely: oxidation-precipitation, filtration, lime softening, ion exchange e.t.c have been employed for iron removal from underground waters (Wong, 1984; Michalakos et al., 1997 and Twort et al., 2000). The oxidation-precipitation-filtration method is the preferred method in most developing and developed countries because it is more economical and less complicated (Sogaard et al., 2000). In oxidation-precipitation-filtration method, two basic physicochemical mechanisms are involved (Rott, 1985), namely, oxidation floc formation and absorption-oxidation mechanisms (Sharmer et al., 2005). Both mechanisms occur simultaneously in most conventional iron removal plants. However, under certain conditions, the dominant mechanism depends on the water quality and process conditions applied.

In this research work, we report the physicochemical properties of dug well waters in Okada town and its environs with a view to determine the extent of

*Corresponding author. E-mail: chikeorjiekwe@yahoo.com. Tel: +2348066413048.

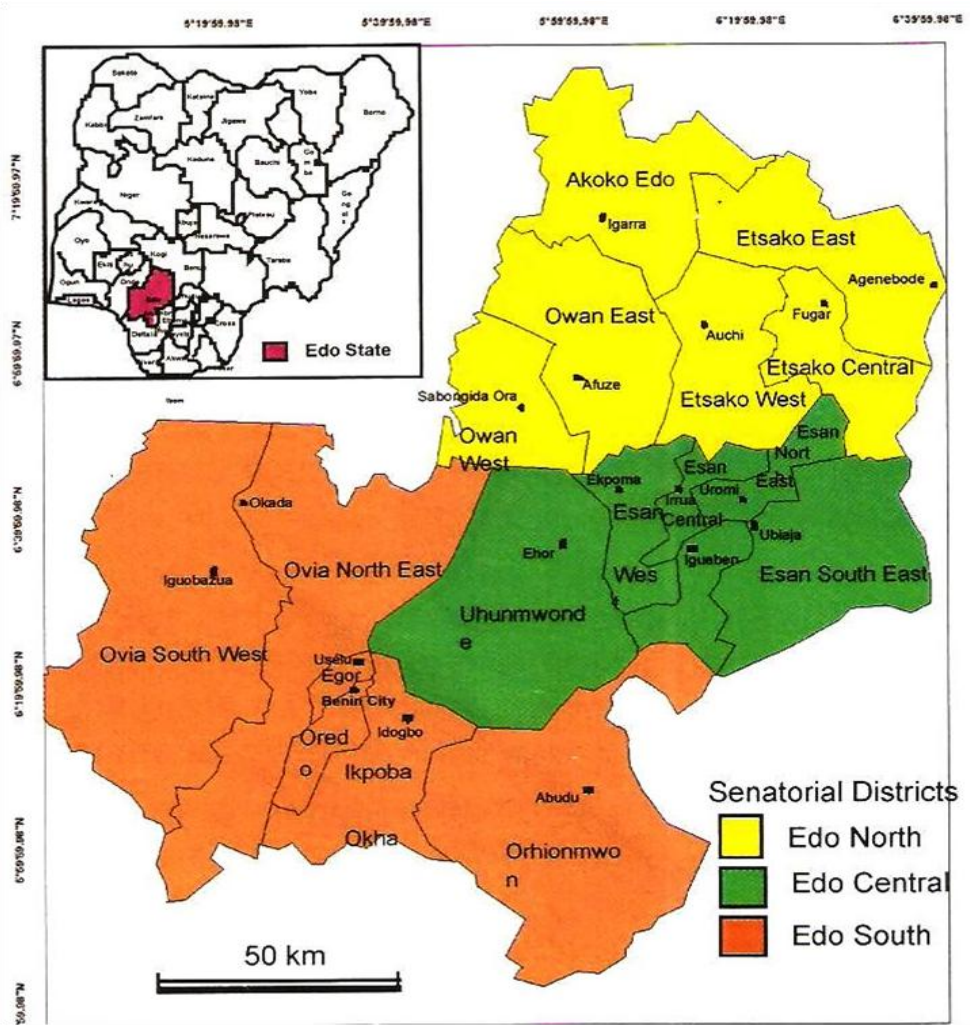

Figure 1. Edo state senatorial districts.

pollution. Also included is the novel method of iron removal from the dug well waters by treatment with sodium hydroperoxide.

MATERIALS AND METHODS

Apparatus

The equipments used were Celsius thermometer (0-100°C), pH meter scale, Gooch funnel, oven, filter papers and flasks, conductivity cell, Hach colorimeter, Atomic Absorption spectrophotometer, 200 litre pressure tank, Electric motor mixer, water pump, vacuum pump, Calcite filter and storage tank.

Reagents

The reagents used for this study were purchased from Aldrich Chemical Company. They are all of analytical grades and were used directly without further purification. They include hydrogen peroxide, H_2O_2, sodium carbonate, Na_2CO_3 and distilled water.

Sampling area

25 underground dug well water were randomly selected and sampled within five communities in Ovia North-East Local Government area of Edo State. These are labeled DW_1 to DW_{25}. The map of the sampled area is shown in Figures 1 and 2.

Physicochemical properties

The measurement of temperature, pH, conductivity, TDS, TSS, total hardness, colour, turbidity, nitrate, phosphate, dissolved oxygen, calcium, magnesium, iron and manganese ion in the dug well water samples were carried out according to previously reported standard methods (Ademoroti,1996 and Chike et al., 2006).

Treatment of water samples with sodium hydroperoxide

About 180 L of dug well water was taken into the pressure tank with the aid of a water pump. 50% H_2O_2 solution and 2 M Na_2CO_3 solutions was prepared from the stock samples provided. 30 ml of 50% H_2O_2 and 5 ml of 2M Na_2CO_3 were mixed together in a beaker

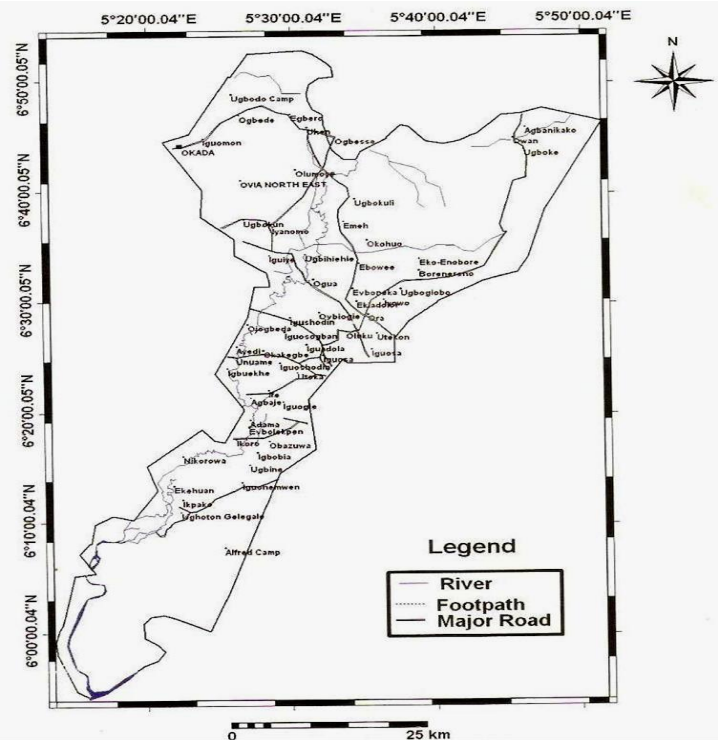

Figure 2. Map of Ovia North-Esat Local Government Area.

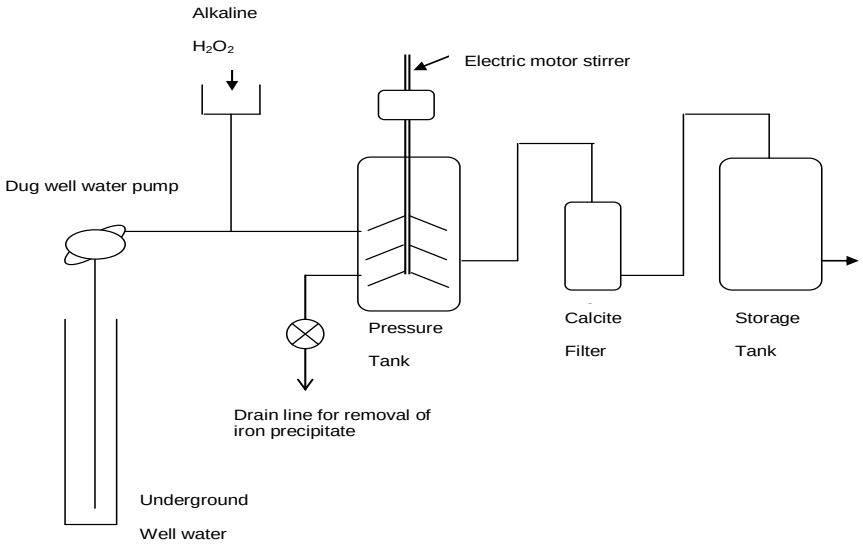

Figure 3. Iron removal by treatment with sodium hydroperoxide.

and allowed to stand for about 3 min to generate sodium hydroperoxide, NaOOH which is the oxidant. The NaOOH mixture was then poured into the tank and stirred with the aid of electric motor mixer for about 1 min. There was immediate precipitation of ferric hydroxide, Fe $(OH)_3$. This was consequently allowed to settle for about 30 min, filtered and stored in the storage tank before distribution, (Figure 3).

RESULTS AND DISCUSSION

The results of the physiochemical characteristics of dug well water samples from Okada town and other surrounding community is presented in Table 1. The temperature of the dug well water samples ranged from

Table 1. Results of physicochemical properties of dug well water samples from Okada Town and its environs.

Community	Dug well Water sample	Temp. (°C)	pH	Δm (ms/cm)	TDS (mg/L)	TSS (mg/L)	Total hardness (mg/L)	Ca (mg/L)	Mg (mg/L)	Fe (mg/L)	Mn (mg/L)	Colour (Pt Co)	Turbidity (fau)	Nitrate (mg/L)	Phosphate (mg/L)	(DO) (mg/L)
Iguomon	DW_1	28.19	7.06	88	44	56	36	28	8	5.8	1.8	334	93	0.15	0.09	5.20
	DW_2	28.10	7.10	90	50	54	36	27	8	6.0	2.0	324	88	0.13	0.08	5.40
	DW_3	28.00	6.90	94	55	55	40	26	9	6.2	1.6	320	86	0.20	0.09	5.50
	DW_4	28.10	7.10	90	50	56	40	27	9	5.8	1.8	324	84	0.14	0.10	5.30
	DW_5	28.10	7.06	90	45	57	36	28	8	6.0	2.0	340	95	0.16	0.10	5.30
Ogbese	DW_6	28.05	6.90	45	23	13	18	14	4	4.0	1.4	12	16	0.18	0.06	4.76
	DW_7	27.90	7.00	44	22	12	16	12	5	4.2	1.2	13	15	0.17	0.07	4.90
	DW_8	27.80	7.10	40	22	11	17	13	6	4.4	1.6	13	17	0.17	0.06	4.90
	DW_9	27.90	7.00	44	24	14	17	12	5	4.2	1.2	13	16	0.18	0.07	4.70
	DW_{10}	28.10	6.90	46	23	13	18	14	4	4.0	1.4	12	15	0.20	0.08	4.80
Okada	DW_{11}	28.28	7.35	198	99	10	70	50	20	8.0	2.6	22	16	0.09	0.06	5.19
	DW_{12}	27.90	7.20	182	90	14	68	49	21	7.8	2.4	21	15	0.08	0.05	5.20
	DW_{13}	28.00	7.45	170	85	12	66	48	22	8.4	2.8	24	15	0.11	0.07	5.30
	DW_{14}	27.90	7.30	183	90	14	67	51	20	8.4	2.4	21	16	0.10	0.06	5.10
	DW_{15}	28.30	7.20	190	100	12	72	49	21	7.8	2.6	23	18	0.09	0.05	5.20
Uhen	DW_{16}	28.17	6.89	96	48	119	42	31	11	6.0	2.0	495	184	0.12	0.07	5.21
	DW_{17}	28.00	7.00	88	45	124	40	29	12	6.2	1.8	490	180	0.11	0.06	5.30
	DW_{18}	27.90	7.10	84	40	130	39	30	13	6.4	2.2	500	190	0.14	0.08	5.40
	DW_{19}	28.00	7.00	86	46	123	40	32	12	6.0	2.0	490	182	0.12	0.07	5.10
	DW_{20}	28.20	6.90	94	50	120	41	29	12	6.2	1.8	492	188	0.13	0.07	5.30
Utese	DW_{21}	28.19	7.07	46	23	8	18	12	6	4.0	1.4	7	14	0.12	0.06	5.20
	DW_{22}	28.10	7.20	55	22	7	19	13	7	3.8	1.2	7	13	0.13	0.04	5.20
	DW_{23}	28.00	6.90	45	20	9	20	14	6	4.4	1.4	8	15	0.14	0.05	5.30
	DW_{24}	28.10	7.20	56	22	7	18	12	7	4.2	1.2	7	14	0.11	0.05	5.10
	DW_{25}	28.20	7.10	60	24	10	18	13	8	4.0	1.6	7	14	0.12	0.06	5.30
WHO		24.50-8.80	6.50 - 8.00	< 10	< 6	< 2	< 100	< 75	< 25	0.3	0.05	< 500	< 0.1	< 0.3	< 0.10	> 100

Table 2. Iron and manganese content of the dug well water samples before and after treatment With NaOOH.

Communities	Dug well water sample	Fe and Mn content before treatment with NaOOH		Fe and Mn Content after treatment with NaOOH	
		Fe (mg/L)	Mn (mg/L)	Fe (mglL)	Mn (mg/L)
	DW_1	5.8	1.8	0.15	0.02
	DW_2	6.0	2.0	0.18	0.03
	DW_3	6.2	1.6	0.20	0.02
Iguomon	DW_4	5.8	1.8	0.20	0.03
	DW_5	6.0	2.0	0.15	0.03
	DW_6	4.0	1.4	0.10	0.02
	DW_7	4.2	1.2	0.15	0.02
	DW_8	4.4	1.6	0.15	0.03
Ogbese	DW_9	4.2	1.2	0.10	0.02
	DW_{10}	4.0	1.4	0.15	0.03
	DW_{11}	8.0	2.6	0.20	0.03
	DW_{12}	7.8	2.4	0.15	0.02
	DW_{13}	8.4	2.8	0.20	0.03
Okada	DW_{14}	8.4	2.4	0.15	0.02
	DW_{15}	7.8	2.6	0.20	0.03
	DW_{16}	6.0	2.0	0.15	0.02
	DW_{17}	6.2	1.8	0.10	0.02
	DW_{18}	6.4	2.2	0.10	0.03
Uhen	DW_{19}	6.0	2.0	0.09	0.03
	DW_{20}	6.2	1.8	0.09	0.04
	DW_{21}	4.0	1.4	0.10	0.03
	DW_{22}	3.8	1.2	0.08	0.03
	DW_{23}	4.4	1.4	0.10	0.03
Utese	DW_{24}	4.2	1.2	0.10	0.02
	DW_{25}	4.0	1.6	0.09	0.02
WHO		0.3	0.05	0.3	0.05

27.8 - 28.3 °C which is within the acceptable range recommended by World Health Organization (WHO). The maximum allowable limit for pH by WHO for safe drinking water is 6.50 - 8.00. The pH of all the dug well water samples also fell within this range. The conductivity of the water samples is a measure of the dissolved ions in the water.

Dug well water samples from Okada have the highest conductivity values, which corroborate its highest values for Ca, Mg, Fe and Mn ions. Dug well water samples from Uhen community has the highest average TSS value of about 123 mg/L which surpassed the WHO guideline value of 2.0mg/L for TSS. This corroborates very well with the highest average values of 495 PtCo and 185mg/L measured for colour and turbidity respectively. All the dug well water samples from the five communities contain Fe and Mn exceedingly in nuisance quantity far above the WHO allowable limit. Dug well water samples from Okada community have the highest values. The results were expected considering the fact that the soil from these areas is mostly laterite, with high iron content. Therefore the iron must have got into the underground water through leaching and seepage from the soil. The high content of Fe and Mn ions has obvious deleterious consequences on the use of the dug well waters for both domestic and drinking purposes. Such consequences include bad taste, staining and browning of clothes, food, containers and skin.

In this regard, a pretreatment procedure is advocated for the dug well water to bring the concentration of Fe and Mn to a tolerable level. Table 2 shows the content of Fe and Mn of the dug well water samples after treatment with sodium hydroperoxide and NaOOH. The dug well water was clear when drawn but gradually turned brown

due to precipitation of ferric hydroxide and $Fe(OH)_3$ caused by atmospheric oxidation of the dissolved ferrous iron. The result indicates that the iron is present mostly as dissolved ferrous bicarbonate and $Fe(HCO_3)_2$. After treatment, the iron and manganese concentrations in the dug well water samples are considerably reduced to below 0.2 and 0.04 mg/L respectively. These values are tolerable concentration level for these ions since they fall within the WHO allowable limits.

The Na_2CO_3 solution was used to generate the sodium hydroperoxide, which is the powerful oxidant (Equation 1). The sodium hydroperoxide decomposes insitu to generate oxygen atom, [O] which then oxidizes the iron (II) to insoluble iron (III) (Equations 2 and 3).

The following mechanistic steps have been suggested for the reaction:

$$Na_2CO_3 + 2H_2O_2 \longrightarrow 2NaOOH + CO_2 + H_2O \quad (1)$$

$$2NaOOH \longrightarrow 2NaOH + 2[O] \quad (2)$$

$$Fe^{2+} + 3/2[O] + 3/2H_2O \longrightarrow Fe(OH)_3 \quad (3)$$

The overall equation of the reaction is therefore given by equation below:

$$2Fe(HCO_3)_2 + ½O_2 + H_2O \rightarrow 2Fe(OH)_3\downarrow + 4CO_2\uparrow \quad (4)$$

The ebullition of hydrogen peroxide aids the coagulation of the suspended ferric hydroxide particles. Apart from iron removal, this method is particularly better than most conventional methods for the following reasons:

(1) The hydrogen peroxide, H_2O_2 is a very important powerful germicide and is capable of disinfecting the water.
(2) The reaction is very fast and cost effective since reaction is completed in a few minutes and just about 35ml of the NaOOH mixture is required per 180 L of raw water (cf. 1Kg of Calcium hypochlorite per 100 Kg of raw water)
(3) It is environmentally friendly when compared with other conventional methods such as chlorination or ozonation e.t.c.
(4) It does not require external coagulant.

Conclusion

Raw water from dug wells from Okada town and neighbouring communities have very high iron concentration because of the high iron content of the laterite soil. Treatment with alkaline hydrogen peroxide is one surest way of removing dissolved iron from underground dug well or borehole waters. The method is preferable than most conventional methods because it is fast, cost effective, environmental friendly and does not require external coagulant.

ACKNOWLEDGEMENT

The Authors acknowledge the financial assistance of Igbinedion University management and the Marine Research Institute of Oceanography, Lagos, Nigeria for the use of their Analytical Laboratory.

REFERENCES

Ademoroti CMA (1996). Standard Methods for Water and Effluent Analysis. Foludex Press Ltd., Ibadan, Nigeria, pp. 20-30.
Machmeier RE (1971). Iron in Drinking Water. University of Minnesota Agricultural Extension Services. pp. 2–5.
Masters GM (1998). Introduction to environmental Engineering. 2ND Edition, Upper Saddle River, NJ: Prentice Hall pp. 11–12
Michalakos GD, Nieva JM, Vaynes DV, Lybertos G (1997). Removal of iron from potable water using trickling filter. J. Water Res. 31(5):991-995
Chike OL, Oshin D, Orjiekwe IU (2006). Water quality index assessment of Evebonede and Ovia Rivers in Ovia North-East LGA of Edo State, Nigeria. Int. J. Chem. 16(4):223 - 228
Rott U (1985). Physical, chemical and biological aspects of the removal of iron and manganese underground. J. Water Supply. 3(2):143-150
Sharmer SK, Petrusevski B, Schippers JC (2005). Advance ground water treatment: iron, manganese, fluoride and boron removal. J. Water Supply: Res. Technol. 54(4):239–244.
Sogaard EG, Modenwaldt R, Abraham-Peskir JV (2000). Conditions and rates of biotic and abiotic iron precipitation in selected fresh water plants and microscopic analysis of precipitate morphology. J. Water Res. 34(10):2675-2682.
Twort AC, Ratnayaka DD, Brandt MJ (2000). Standards for physical and chemical quality of water supply. 5TH Ed. Arnold London. pp. 4-46.
WHO (1996). Guidelines for Drinking Water Quality. Health Criteria and other supporting information, 2ND Ed., WHO Geneva.
Wong JM (1984). Chlorination-filtration for iron and manganese removal. J. Am. Water Works Assoc. 76(1):76 –79.

academicJournals

Vol. 8(28), pp. 1470-1480, 30 July, 2013
DOI: 10.5897/IJPS2013.3927
ISSN 1992 - 1950 © 2013 Academic Journals
http://www.academicjournals.org/IJPS

International Journal of Physical Sciences

Full Length Research Paper

Assessment of leachate effects to the drinking water supply units in the down slope regions of municipal solid waste (MSW) dumping sites in Lahore Pakistan

Khalid Mahmood[1], Syeda Adila Batool[1], Asim Daud Rana[1], Salman Tariq[1], Zulfiqar Ali[2,3]* and Muhammad Nawaz Chaudhry[2]

[1]Department of Space Science, University of the Punjab, Lahore, Pakistan.
[2]College of Earth and Environmental Sciences, University of the Punjab, Lahore, Pakistan.
[3]Nano Science and Catalysis Division, National Centre for Physics, Q.A.U Campus, Islamabad, Pakistan.

Accepted 30 July, 2013

The aim of this study was to evaluate seasonal as well as moderate temporal effects on deep groundwater quality by the dumpsites leachate in the Lahore Metropolitan with a population of about 8 million. Groundwater samples for this study ware drawn from groundwater supply units installed by local government for the provision of drinking water to the residents. The groundwater in down slope regions from municipal solid waste (MSW) dumping sites has been identified by using Inverted Watershed technique. Eleven water supply units have been spotted that fall within the identified leachate plumes. Parameters of pH, turbidity, electric conductivity, total dissolved solids (TDS) and *Escherichia coli* were determined on water samples from these identified units. The quality analysis indicates that the effect of the leachate is more prominent in the hot and dry pre-monsoon season due to the domination of base flow for recharge of the groundwater, whereas dilution observed in leachate contamination during and immediately after the monsoon rainy season is due to the recharge through seepage of the rain water which dominates the base flow. Variation in the correlation factor between electric conductivity and TDS has been used to estimate constituents of TDS contributed both by rainfall seepage and base flow. An increasing tendency, showing influence of the leachate on the deep water quality, has been observed while analyzing the correlation between distance of the tube wells from leachate sources and measurements of quality parameters.

Key words: Base flow, deep groundwater, down slope regions, landfill leachate, rainwater seepage.

INTRODUCTION

Almost 70% of the earth is covered with water but only 2.5% of this is fresh water (PCRWR, 2007; Limouzin and Maidment, 2009) is suitable for human use. Approximately 99% of fresh water is in aquifers (ESA, 2001; Gabriel and Khan, 2010) and being used as the major source of drinking water in Pakistan. Lashari et al. (2007) estimated that about 60 to 70% population of Pakistan depends directly or indirectly on groundwater for their livelihood. However, a number of locations in Punjab province of Pakistan have been reported to be contaminated by by-products of waste materials (World Bank, 2006). Therefore, qualitative and quantitative monitoring of these fresh water reservoirs is mandatory for human health.

Underlying aquifer is the main source of water for the city of Lahore like the rest of the Punjab province with a population of 80 million. The extraction of this groundwater can be categorized in three types depending

*Corresponding author. E-mail: zali1964@hotmail.com. Tel: +92301-5551014. Fax: +92-512077395.

on depths. The first category ranges in depth from 9 to 18 m depending upon the aquifer level. This serves the poor households around the dumpsites and cottage industry. The second category serves the agriculture; the water is drawn by relatively large water extraction tube wells with almost the same depth range as for the first category. The third type of extraction wells are installed by government agencies for the provision of drinking water to residents of the city. These tube wells are considered most sophisticated and deepest (150 to 180 m).

Provision of water supply to about 90% population of Lahore is the responsibility of Water and Sanitation Agency (WASA), which has installed over 450 tube wells and given over 531,336 connections in the city (Gabriel and Khan, 2006). Other agencies like Lahore Cantonment Board, Model Town Society etc. serve the remaining 10% population of Lahore. Gabriel and Khan (2006) reported that these tube wells are of varying capacity and are operated for an average duration of 16 to 18 h a day and the depth of these tube wells, varies from 150 to 180 m. Hydro-geologically, Lahore is a part of large interfluvial Bari Doab, bounded by River Ravi to the north-west and Rivers Satlej and Beas to the south-east. Its aquifer is un-confined with a thickness of about 400 m (Gabriel and Khan, 2006) and is composed predominantly of fine to medium grained sands and small lenses of silty clay.

Monitoring of underlying aquifer in the vicinity of a dumping site is mandatory for the protection of groundwater. Dumping sites provide an easy and the cheapest way for waste management all over the world (Mahini and Gholamafard, 2006; Zhang et al., 2011; Butt et al., 2008). However, without properly designed and maintained, microbial and chemical products from the dumping site may produce harmful effect to the environment (Butt and Oduyemi, 2003). Hazards associated with landfills require proper evaluation even after their construction, in order to estimate and eradicate the bad effects to environment and public health (Gorsevski et al., 2012). Contamination of the underlying aquifer by leachate from the dumping sites is the most highlighted environmental issue found in the reviewed literature (Butt and Oduyemi, 2003; Santos et al., 2006; Demitriou et al., 2008; Din et al., 2008; López et al., 2008; Singh et al., 2009; Li et al., 2012). For examples, groundwater contamination near the Ano Liosia landfill was reported in Attica region, Greece, which was unsuitable for irrigation (Feta et al., 1996). Another example is in Delaware New Castle where wells located downstream of the Llangollon landfill were found to be heavily contaminated and subsequently abandoned (Chian and DeWalle, 1976).

In 2009, the areas under the jurisdiction of Lahore city produced about 5000 tons/day of municipal solid waste (MSW), where 60% of the waste was collected and disposed of in the open dumpsites (Batool and Chohdary, 2009). Two major sites for municipal waste dumping in Lahore are located in Saggian and Mahmood Booti as shown in Figure 1. These dumping sites have neither a leachate collection system nor an impermeable liner system. The dumpsite leachate percolates through underlying sediments and contaminates the source of drinking water (Biswas et al., 2010; Li et al., 2012). Once the groundwater is contaminated, they are unable to be cleaned to a level that can meet international drinking water quality standards (Biswas et al., 2010). Horizontal spread of percolated landfill leachate is very limited (Cherry, 1990) but it moves down slope as a wide front of contamination (Lee and Lee, 1993). Municipal landfill's leachate is heavier than groundwater, therefore, after percolation through lithological cross section it will sinks to the depth where it is diluted to a level where its density becomes comparable to that of the uncontaminated groundwater (Cherry, 1991; Lee and Lee, 1993).

In the pre-monsoon season, lateral flow of groundwater is dominant while in the post-monsoon, vertical flow dominates the groundwater recharge. Lateral flow brings contamination to a location from its neighboring sources and the vertical flow brings contamination from the location itself. Most of the studies that analyzed the leachate hazards to the groundwater had used shallow (1 to 10 m below surface) water samples, where the effects are more pronounced (Jensen et al., 1998; Nyenje et al., 2013). This study is intended to delineate down slope groundwater regions of Mahmood Booti and Saggian dumping sites and the quality assessment of the drinking water supply tube wells that are located within the identified hazardous zones. The groundwater sampling depth ranges from 79 to 137 m from the tube wells installed by the government for the provision of drinking water. Timely detection of groundwater pollutants may lead to remedial measures for sustainability of the drinking water source. For this purpose some indirect methods have been used for the analysis of contamination caused by leachate to these depths.

MATERIALS AND METHODS

Methodology for this study has been divided into two steps. In the first step, down slope groundwater areas of each landfill have been identified and hence delineated. Afterward, in the second step tube wells falling within this area were assessed for the quality of drinking water.

Down slope area identification

WASA periodically measures the depth of groundwater on each of its tube wells installed within Lahore district. For this study, static water level (SWL) values for the months of April, July and October from 2009 to 2011 were used. Geo-referencing of the tube well sites was accomplished by a field survey identifying each tube well site using Garmin GPS map 76CSx with an accuracy of ±3 m. In order to develop water table, the point measurements had been interpolated after comparison of many techniques available for interpolation as shown in Table 1. This comparison had optimized Kriging (simple kriging) as the most suitable for the interpolation.

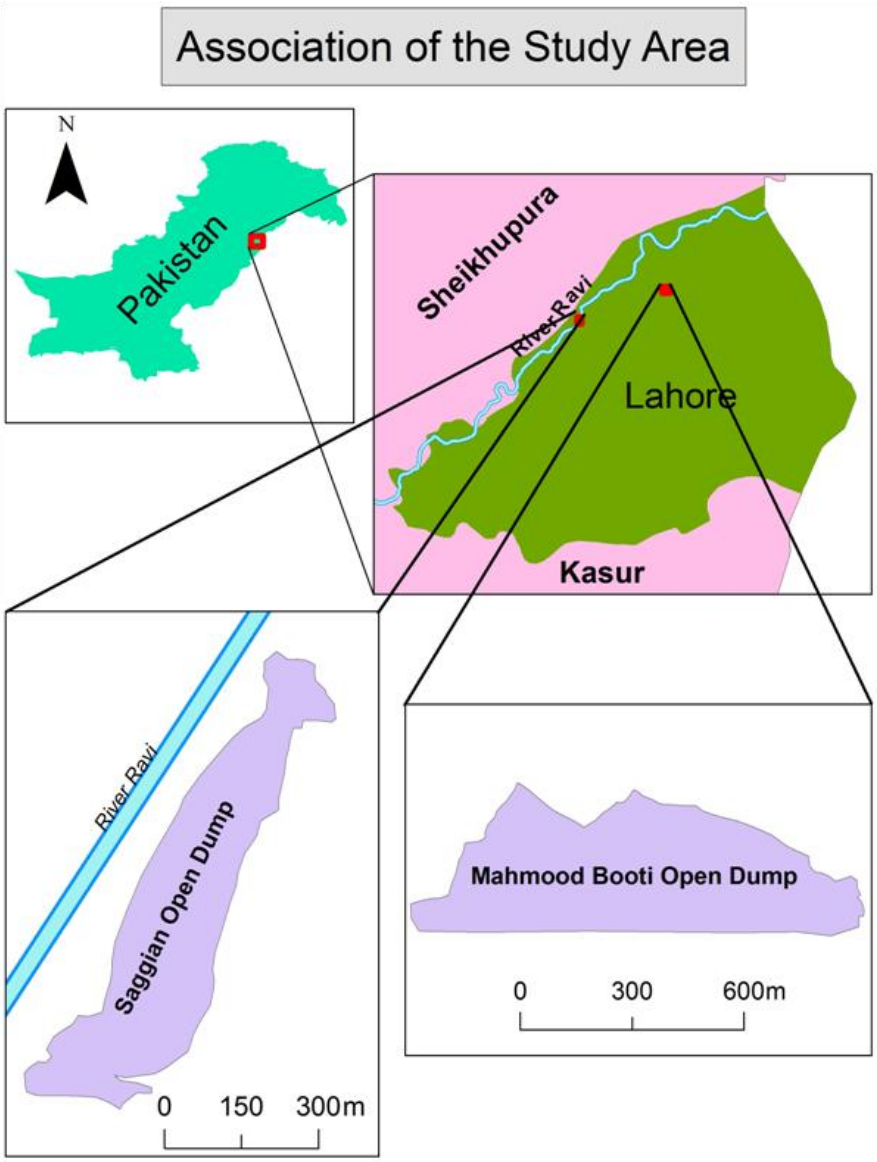

Figure 1. Dumping sites location in Lahore, Pakistan.

Table 1. Comparison of interpolation techniques.

Method	RMSE	Correlation	Mean
IDW	3.492	0.890536	0.1231
Spline	3.399	0.897549	0.1748
Kriging	3.37	0.898589	0.02551

For the down slope area identification some of the geographic information systems (GIS) software only facilitates in finding down slope trajectories for individual pixels; whereas, one of the objectives of the study was to delineate all the area that receives water after passing through the landfills, therefore an indirect approach has been applied for this purpose. The method devised in this study for the down slope area identification is an inverse watershed technique. In this technique, the water table surface is inverted to get its reflection surface which shows higher areas at low levels and vice versa. The down slope areas in the actual raster surface will appear to be up slope areas or in other words, watersheds, in the output surface. The process of inversion of water

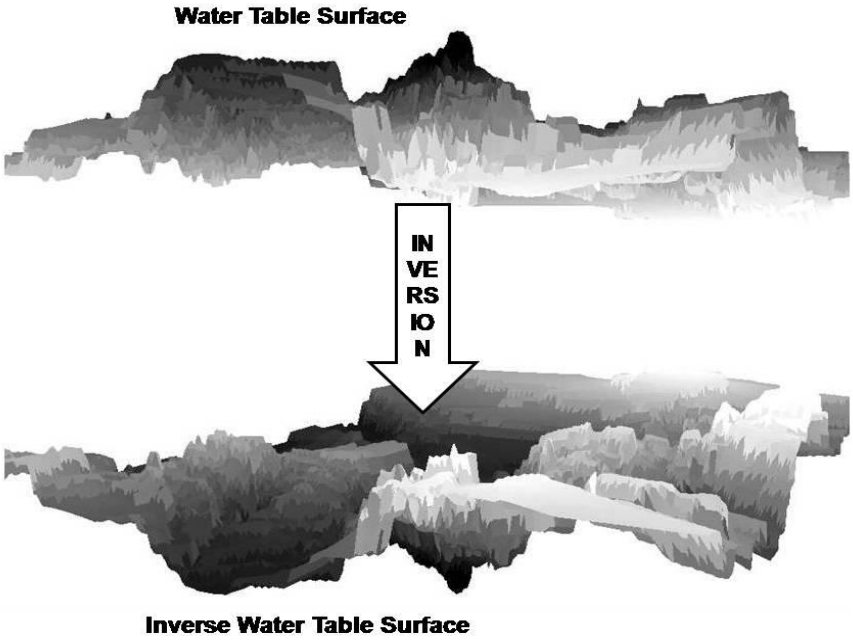

Figure 2. Inversion of groundwater surface.

table surface is shown in Figure 2.

Both landfills were used as target feature for delineating watersheds based on the inverted water table surface. This watershed gives the required down slope regions of the groundwater from landfills. To incorporate possible variations in the down slope area a time series of water table surfaces consisting of nine datasets spanning from April, 2009 to October, 2011 were used in this study. Groundwater surface changes with time as a consequence of rates and position of water extraction and recharge, the combined output of all down slope regions is shown in Figures 3 and 4 for Mahmood Booti and Saggian landfills, respectively. As a hypothesis, the estimated down slope areas from various input surfaces must overlap as they belong to the same region. Therefore, in the final down slope region only those areas which overlapped by at least two of the datasets were selected. The outputs of all the overlapping datasets are united for the demarcation of the down slope areas of both the dumping sites.

Quality assessment of risk prone tube wells

The final down slope area for each of the dumping sites identifies the possible hazardous region prone to leachate contamination. Tube wells installed by WASA, Lahore for drinking water supply were identified in this study. After identification of expected risk prone water supply units, an assessment was performed to check the water quality of these tube wells. The qualitative report of expected risk prone tube wells for pre-monsoon 2010 was taken from WASA, Lahore. The other data set for the water quality assessment was acquired especially for this study in post-monsoon 2012. The available datasets made it possible to provide both seasonal as well as moderate temporal changes in the drinking water quality. This time gap provided a fair chance to evaluate the impacts of leachate, having a slow lateral movement (Cherry, 1990), even at the farthest tube well identified. Water samples of the tube wells were collected in neat, airtight and sterilized polyethylene 500 ml bottles. Samples were immediately brought to laboratory for the analysis of selected water quality parameters.

In the pre-monsoon season, lateral flow of ground water is more dominant, whereas in the post-monsoon season, vertical flow dominates the groundwater recharge. Both seasons were taken into account to determine the influence of lateral as well as vertical flow of recharge to water quality. In order to highlight the influence of landfill leachate to water quality parameters a basic principle of likelihood has been used by virtue of which any effect caused by a source is inversely related to the distance (Nyenje et al., 2013). A correlation of each quality parameter with distance from dumping site was established. The distance from the dumping site had been taken, keeping in view, both the filter depth of tube wells and its ground distance from the dumping sites as shown in Figure 5.

RESULTS AND DISCUSSION

The delineated down slope regions for both municipal dumpsites show a general trend of groundwater flow from dumping sites towards the residential area of the city as shown in Figure 6. The extracted down slope regions using inverse watershed technique are verified by the cited literature, as explained in the following points:

1) It is a fact that almost all the extraction of groundwater for livelihood is made in central portions of the city leading to a depression zone as mentioned by a number of studies (Mahmood et al., 2013). So, in order to maintain surface level, water flows from outer boundaries, beneath municipal dumpsites, to inner regions of the city.

2) The River Ravi exists as one of the major recharge sources of Lahore's groundwater at northern and western edges of the city (Basharat and Rizvi, 2011; Mahmood et al., 2013). Since the leachate producing bodies are

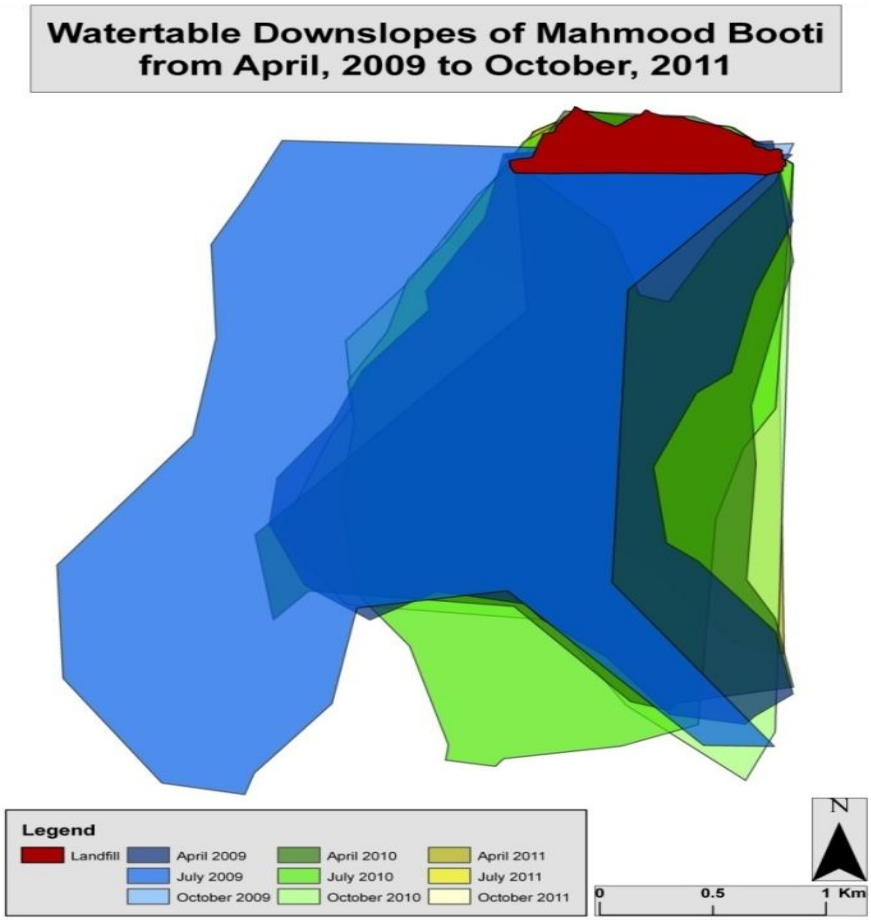

Figure 3. Time series of Water table down slopes of Mahmood Booti dumping site.

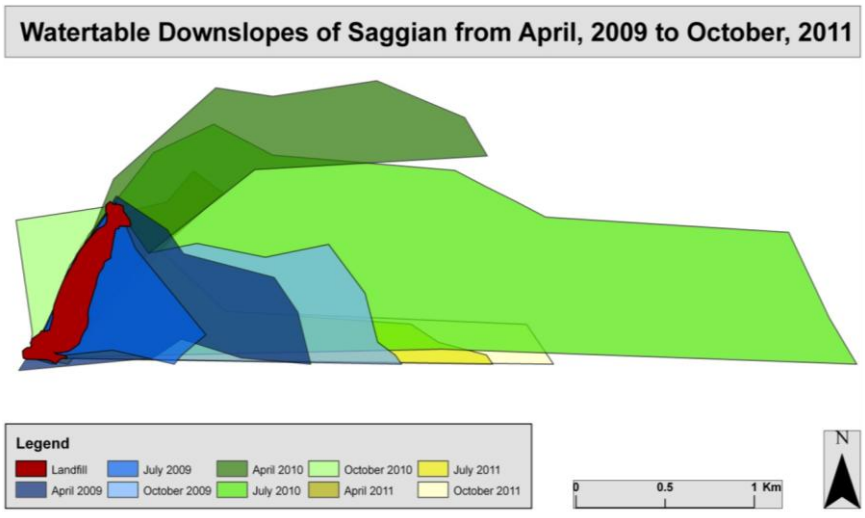

Figure 4. Time series of Water table down slopes of Saggian dumping site.

situated away from River Ravi to the residential part of the city, therefore, flow of the water for recharging the underlying aquifer is from dumpsites to central city. In this way, leachate contaminates that part of the groundwater

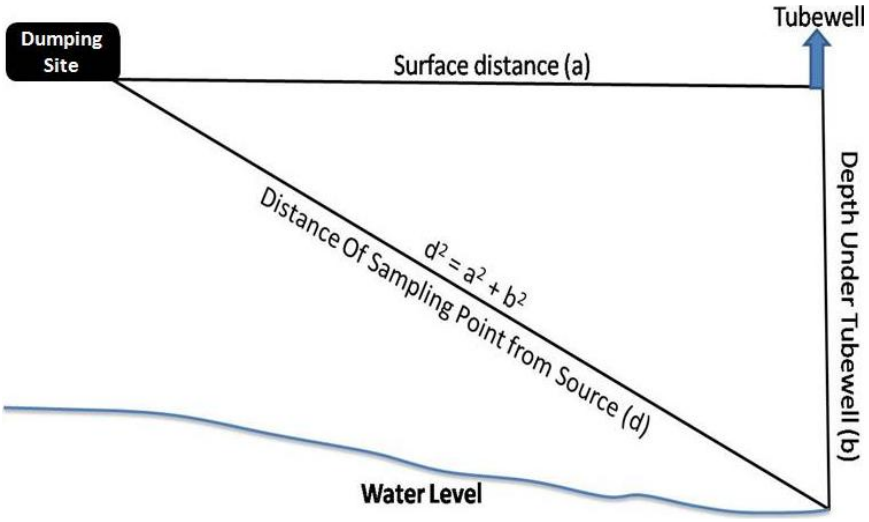

Figure 5. Distance from dumping site to tube well filter

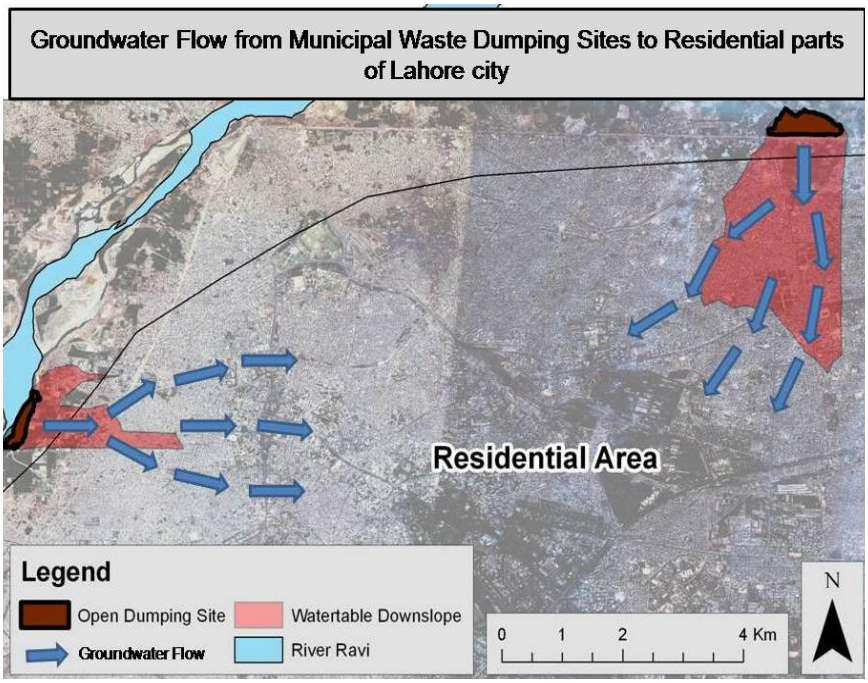

Figure 6. Groundwater flow to the Lahore city.

which has to be ultimately extracted for human usage.

Effects on the drinking water supply units/tube wells

Table 2 lists the details of risk prone tube wells identified in this study. Nine tube wells were located within contamination reaches in Mahmood Booti dumping site (Figure 7) and two tube wells were in the Saggian dumpsite (Figure 8).

The quality parameters for the risk prone tube wells are shown in Table 3. The landfill leachate contains acidic substances that cause decrease in pH value of the leachate (Kareem et al., 2010) which further tends to decrease pH of the ground water if it gets mixed with it. Keeping in view this effect to the pH parameter, Table 3 shows the average measured pH of groundwater is more acidic in the pre-monsoon season than the post-monsoon

Table 2. Tube wells at risk along the dumping sites.

S/N	Serving area	Effecting dumping site	Design capacity (Cusecs)	Distance from landfill (m)	Water depth Nov, 2011(m)	Water sampling depth (m)
1	Madho Lal Hussain	Mahmood Booti	0.112	2565	39.62	137
2	Dy. Yaqoob Colony	Mahmood Booti	0.112	2049	32.92	137
3	Aliya Town	Mahmood Booti	0.112	548	32.69	137
4	Gulshan-e-Shalimar	Mahmood Booti	0.112	1148	32.5	137
5	Angoori Bagh SchemeNo.1	Mahmood Booti	0.056	3172	39.5	137
6	Gosha-e-Angoori	Mahmood Booti	0.112	3190	39.1	137
7	Kotli Pir, Abdul Rehman	Mahmood Booti	0.112	3328	39.8	137
8	Naseer Abad, Pakistan Mint	Mahmood Booti	0.112	2595	39.5	137
9	Mahmood Booti Well Center 3	Mahmood Booti	0.112	50	32.55	137
10	Rafi Abad Darbar	Saggian	0.056	987	23.71	79
11	Islam Pura	Saggian	0.112	2095	25	79

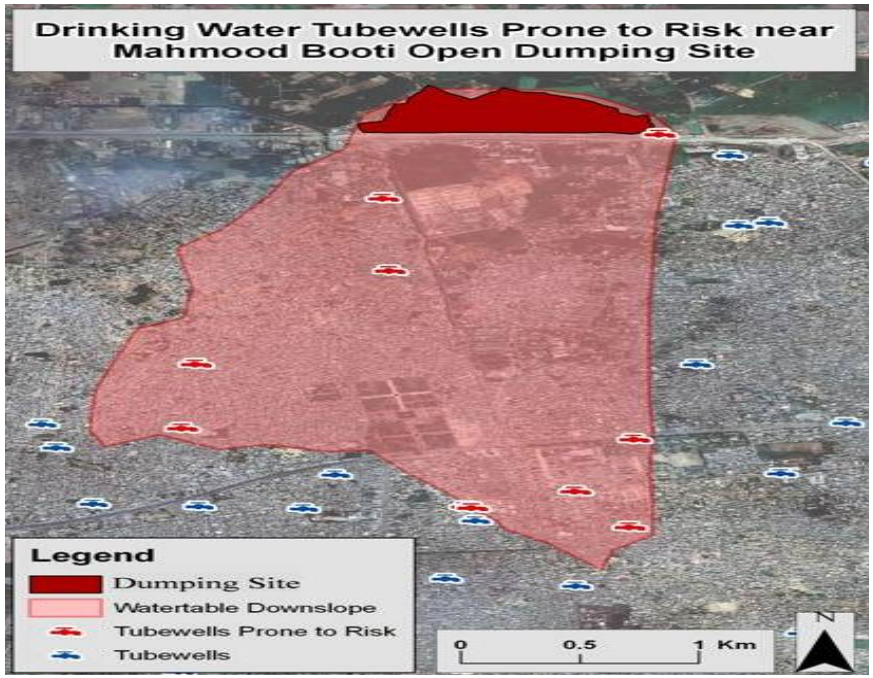

Figure 7. Drinking Water at risk around Mahmood Booti.

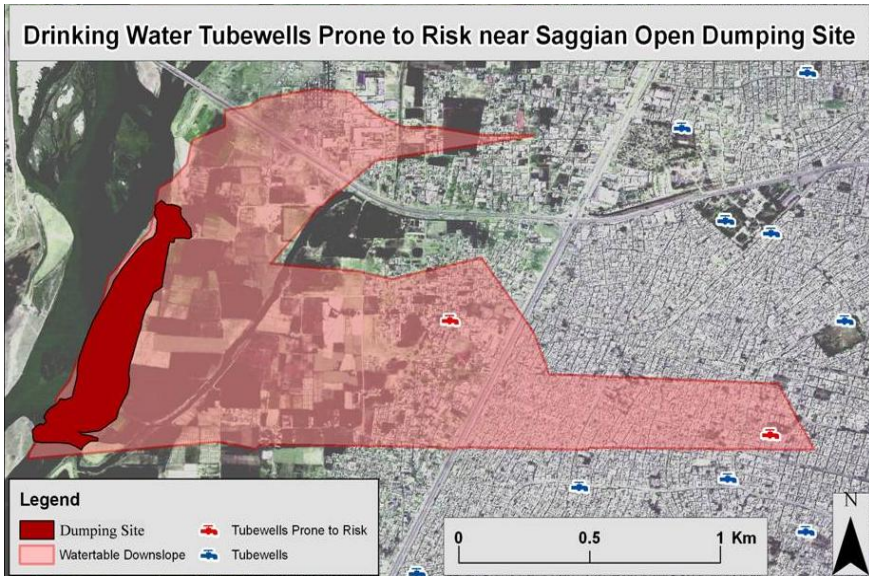

Figure 8. Drinking Water at Risk around Saggian

Table 3. Quality degradation chart of the risk prone tube wells.

S/N	Location	PH		Turbidity (NTU)		Conductivity (ms/cm)		TDS (ppm)		*E. coli*	
		Pre MS*	Post MS*	Pre MS*	Post MS*	Pre MS*	Post MS*	Pre MS*	Post MS*	Pre MS*	Post MS*
1	Madho Lal Hussain	7.6	8.4	0.59	0.08	526	430	331.3	290	Absent	Present
2	Dy. Yaqoob Colony	8.1	8.5	0.16	0.09	518	410	236.3	290	Absent	Present
3	Aliya Town	7.5	8.2	1.07	0.13	514	390	323.8	380	Absent	Present
4	Gulshan -e-Shalimar	8.6	8.6	3.44	0.18	886	380	558.1	390	Absent	Present
5	Angoori Bagh SchemeNo.1	7.5	7.9	1.85	0.15	921	1010	580.2	465	Absent	Present
6	Gosha-e-Angoori	7.8	7.9	3.8	0.15	621	1010	391.2	465	Absent	Present
7	Kotli Pir, Abdul Rehman	7.9	8.2	2.02	0.16	560	560	352.8	390	Absent	Present
8	Naseer Abad, Pakistan Mint	7.9	8.1	1.94	0.21	574	530	361.6	359	Absent	Present
9	Mahmood Booti Well Center 3	7.9	8.1	1.97	0.15	380	450	239.4	310	Absent	Present
10	Rafi Abad Darbar	8	8.8	0.57	0.15	321	260	202.2	285	Absent	Present
11	Islam Pura	7.7	8.5	1.67	0.18	392	290	246.9	210	Absent	Present
Averages		7.8	8.2	1.73	0.15	564.8	520	347.6	348.5	Absent	Present

*MS- Monsoon.

Table 4. Change in co-relation (Pearson's r test) among quality parameters.

Correlation between	Pre-monsoon	Post-monsoon
Electric conductivity/TDS	0.97638	0.82374
Electric conductivity/Turbidity	0.511273	0.05530
TDS/Turbidity	0.589632	0.16959
Electric conductivity/pH	0.316727	0.82572
TDS/pH	0.316727	0.68812

measurement. This trend shows the effect of leachate intrusion to be more prominent in pre-monsoon season. As mentioned earlier, the groundwater recharge of the Lahore district is contributed by two main sources; one is the River Ravi and the other is rainfall. The measurement of pH in the pre-monsoon season is more influenced by base flow which carries the effects of the leachate to the groundwater down slope. In the monsoon season groundwater gets the dominant share of its recharge from rainwater that seeps down. In this way, quality of the groundwater is more influenced by the local circumstances. High value of pH in post-monsoon analysis indicates that the decreased value of pH in the pre-monsoon could possibly be due to the leachate, which is diluted in post-monsoon, affecting the increase in pH because of the local influence.

A similar trend is observed in the measurements of turbidity which shows an average decrease from 1.73 to 0.15 NTU. Landfill leachate tends to increase electrical conductivity (Kareem et al., 2010), therefore its value must be higher in the pre-monsoon as compared to the post-monsoon. The measurements (Table 3) agree with the hypothesis, though the effect has not been found as prominent as it was in the cases of pH and turbidity parameters. According to the cited literature, wherever hydrocarbon degradation takes place, it tends to increase total dissolved solids (TDS) (Atekwana et al., 2004). Kareem et al. (2010) has measured high concentration of TDS in the leachate for the same study area. With reference to his study, pre-monsoon measurement of TDS should be higher than the post-monsoon measurements as in this season effect of leachate is diluted considerably as found for other quality parameters, whereas, behavior of TDS is found somewhat variant from the expected, as it has shown an increasing trend from 347.62 to 348.54 ppm.

This anomaly may also be the result of the local geochemical heterogeneity which is more prominent in the post-monsoon season. However, another interesting behavior has been identified in the relation between electrical conductivity and the amount of TDS. Nowaday's electric conductivity is used as a proxy for the measurement of TDS in the water (Post, 2012), based on the assumption that almost all TDS constituent participate in increasing conductivity of the groundwater (Atekwana et al., 2004). In fact, the groundwater contains both the charged and the uncharged species in proportions that may vary depending upon geochemical heterogeneity. For example, dissolved silica (H_4SiO_4) and organic substances do not contribute to increase electric conductivity (Post, 2012). Any increase in uncharged substances disturbs the correlation between the two quantities. Therefore, electric conductivity cannot be directly used for the measurement of TDS, but it only gives a good approximation of the TDS through the relation given by Lloyd and Heathcote (1985):

$$TDS = K_c \times EC$$

Where EC is electrical conductivity and K_c is correlation factor that may vary depending upon proportion of charged and uncharged constituents (Atekwana et al., 2004).

Decrease in the correlation between electrical conductivity and TDS in the post-monsoon season as shown in Table 4, indicates that base flow contribution to the TDS are dominated by charged species for the contributing leachate (Kareem et al., 2010). Whereas decrease in correlation factor and increased TDS in the post-monsoon season reflect that contribution of local influences to TDS is dominated by uncharged species. The charged species may include inorganic substances which may also contain metals for groundwater pollution (Rivett et al., 2011). Changes in the correlation may also be used as an indicator of raising the metal contents in groundwater due to intrusion of the leachate which is one of the serious issues of groundwater contamination (Jensen et al., 1998; Baumann et al., 2006; Malana and Khosa, 2011).

Increase in the effects of leachate to groundwater has also been assessed in terms of correlation of the measured parameters with distance of sampling depths from dumping sites as shown in Table 5.

With reference to Table 5 almost all the parameters had shown increase in the leachate influence over the time except turbidity. The smallest rise is found in the correlation of TDS with the distance, it may be the result of TDS contribution by factors other than the leachate, which already had been explained. Looking at the influential trends over pH and electric conductivity, the effect is almost doubled in the time gap of sampling. Here, it is very important to keep in mind that the samples

Table 5. Changes in influence of leachate over water quality.

S/N	Quality parameter	2010	2012
1	pH	0.25382	0.41689
2	Turbidity	0.20550	0.02893
3	Conductivity	0.39163	0.63782
4	TDS	0.37129	0.38575

Table 6. Additional water quality parameters.

S/N	Location	T.H	Ca	Mg	Cl	HCO_3
1	Madho Lal Hussain	140	35.2	12.4	18	156
2	Dy. Yaqoob Colony	140	35.2	22.4	19	144
3	Aliya Town	176	40	18.2	16	154
4	Gulshan -e-Shalimar	102	19.2	12.9	70	100
5	Angoori Bagh SchemeNo.1	250	48.8	30.7	42	246
6	Gosha-e-Angoori	120	24	14.4	27	172
7	Kotli Pir, Abdul Rehman	140	26.4	17.7	30	188
8	Naseer Abad, Pakistan Mint	120	24.8	15.3	21	166
9	Mahmood Booti Well Center 3	136	28.8	15.3	14	122
10	Rafi Abad Darbar	140	27.2	17.2	10	92
11	Islam Pura	124	24.8	14.8	18	130
Averages		144.36	30.4	17.39	25.91	151.82
Correlation with distance		0.1811	0.10047	0.2589	0.16906	0.72278

in 2012 had been taken after monsoon that had diluted the effects of base flow but the results are still alarming. Other parameters like total hardness (TH), Calcium (Ca), Magnesium (Mg), Chlorine (Cl), and Bicarbonates (HCO_3) can also be used for groundwater quality measurement (Malana and Khosa, 2011) and their source may also be associated with dumping of MSW (Xing et al., 2013). These parameters had also been analyzed in the first dataset taken from WASA, Lahore and are given in Table 6.

Regarding these additional water quality parameters two observations are important to note. The first one is the tube well installed at Angoori Bagh Scheme No. 1 with comparatively high values of all quality parameters. At the second place, the correlation of bicarbonates (HCO_3) with distance from dumping site is high, which shows contribution of leachate to this quality parameter.

CONCLUSION AND RECOMMENDATION

The Inverse Watershed technique had been found fruitful for the identification of contamination plume under Municipal Waste Dumping sites as the results agree with the reviewed literature. Flow of groundwater under both sites is found towards the residential part of the city, which proves unsuitability of locations of the dumping sites. The groundwater in the down slope region around Mahmood Booti has nine tube wells that are being used for the provision of drinking water to residents. Similarly, the leachate plume detected around Saggian dump contains two tube wells of the same kind.

Hazardous effects of landfill leachate to groundwater has been identified which are more prominent in the pre monsoon season and diluted by the intrusion of rainfall water to it in the post monsoon season. The variation in the correlation factor between electrical conductivity and TDS may possibly be due to the intrusion of metals to the groundwater by the leachate. The quality parameters are well within the range of the drinking water standards for these deep tube wells but the increasing influence of leachate in the down slope regions may turn out to be a big issue in the near future.

Therefore, in future, drinking water supply tube wells should be installed at opposite sides of the groundwater down slope directions for the landfills. As the shallow water is more prone to these risks, so shallow bores in the area for drinking water need to be banned.

ACKNOWLEDGEMENTS

We would like to acknowledge and extend our heartfelt gratitude to Mr. Arif Butt, Director Hydrology, WASA,

Lahore for providing data. We also acknowledge Nano Science and Catalysis Division, National Centre for Physics, Quaid-i-Azam University Islamabad, Pakistan and College of Earth and Environmental Sciences, University of the Punjab, Lahore, Pakistan, for providing us technical and analytical facilities.

REFERENCES

Atekwana EA, Rowe RS, Warkema DD, Legall FD (2004). The Realtionship of total dissolved solid measurements to bulk electrical conductivity in an aquifer contaminated with hydrocarbons. J. Appl. Geophys. 56:281-294.

Basharat M, Rizvi SA (2011). Groundwater extraction and waste water disposal regulations – Is Lahore aquifer at stake with as usual approach. Pakistan Engineering congress, World Water Day. pp. 112-134.

Batool SA, Chohdary MN, (2009). Municipal solid waste management in Lahore City District, Pakistan. Waste manage. 29:1971-1981.

Baumann T, Frushtorfer P, Klein T, Niessner R (2006). Colloid and heavy metal transport at landfill sites in direct contact with groundwater. Water Res. 40:2776-2786.

Biswas AK, Kumar S, Babu SS, Bhattaacharyya JK, Chakrabarti T (2010). Studies of Environmental Quality in and around municipal solid waste dumpsite. Resour. Conserv. Recycling. pp. 129-134.

Butt TE, Lockley E, Oduyemi KOK (2008). Risk assessment of landfill disposal sites- State of the art. Waste Manage. 28:952-964.

Butt TE, Oduyemi KOK (2003). A holistic approach to Concentration Assessment of Hazards in the risk assessment of landfill leachate. Environ. Int. 28:597-608.

Cherry J (1990). Groundwater Monitoring: Some Deficiencies and Opportunities. Hazardous Waste Site Investigationns; Towards Better decision, Proceedings of 10th ORNL Life sciences symposium Gatlinberg, TN, May 1990, Lewis publishers.

Cherry J (1991). Waterloo Center for Ground Water research. University of Waterloo, Ontario, Canada, Personal Communication.

Chian SK, DeWalle FB (1976). Sanitary landfill leachate and their treatment. J. Environ. Eng. 102:411-431.

Demitriou E, Karaozas I, Saratakos K, Zacharias I, Bogdanos K, Diapoulis A (2008). Groundwater risk assessment at a heavily industrialized catchment and the associated impacts on a peri-urban wetland. J. Environ. Manage. 988:526-538.

Din MAM, Jaafar WZW, Obot RMM, Hussain WMAW (2008). How GIS can be a Useful Tool to Deal with Landfill Site Selection. International Symposium on Geoinformatics for Spatial Infrastructure Development in Earth and Allied Scinces.

ESA (2001). Water in a Changing World. Ecological Society of America. J. Issues Ecol. Vol. 9.

Feta D, Pabadopoulos A, Loizidou M (1996). A study on the landfill leachate and its impact on the ground water quality of the greater area. Environ. Geochem. Health. 21:175-190.

Gabriel HF, Khan S (2006). Policy Options for Sustainable Urban Water Cycle Management in Lahore, Pakistan. Proceedings of ERSEC Water Workshop 2006 Beijing, China. pp. 180-202.

Gabriel HF, Khan S (2010). Climate Responsive Urban Groundwater Management Options in a Stressed Aquifer System. IAHS Publications, 338:166-168. ISSN 0144-7815.

Gorsevski PV, Donevska KR, Mitrovski CD, Frizado JP (2012). Integrating multi-criteria evaluation techniques with geographic information systems for landfill site selection: A case study using ordered weighted average. Waste Manage. 32:287-296.

Jensen DL, Ledin A, Christensen TH (1998). Specification of heavy metals in landfill leachate polluted groundwater. Water Resour. 33(11):2642-2650.

Kareem S, Chaudhry MN, Ahmad K, Batool SA (2010). Impact of Solid Waste Leachate on Groundwater and Surface water. General Chem. Soc. Pak. 32(5):606-612.

Lashari B, McKay J, Villholth K (2007). Institutional and Legal Groundwater Management Framework: Lessons Learnt from South Australia for Pakistan. Int. J. Environ. Dev. 4(1):45-59.

Lee GF, Lee AJ (1993). Groundwater Quality Monitoring at lined landfills: Adequacy of Subtitle D Approaches. Report of G. Fred Lee & Associates, El Macero, CA.

Li Y, Li J, Chen S, Diao W (2012). Establishing indices for groundwater contamination risk assessment in the vicinity of hazardous waste landfills in China. Environ. Pollut. 165:77-90.

Limouzin M, Maidment D (2009). Water Scarcity is an Indicator of Poverty in the World. A term project of University of Taxas at Austin.

Lloyd JW, Heathcote JA (1985). Natural in organic Hydro-Chemistry in realtion to groundwater. Clarendon Press, Oxford, England.

López JAR, Hernández JR, Mancilla OL, Diazconti CC, Garrido ML (2008). Assessment of groundwater contamination by landfill leachate: A case in México. Waste Manage. 28:33-39.

Mahini SA, Gholamafard M (2006). Siting MSW Landfills with a Weighted Linear combination Methodology in a GIS Environment. Int. J. Environ. Sci. Technol. 3(4):435-445.

Mahmood K, Rana AD, Tariq S, Kanwal S, Ali R, ALI AH, Tahseen T (2013). Groundwater Levels susceptibility to degradation in Lahore Metropolitan. Sci. Int. 25:123-126.

Malana MA, Khosa MA (2011). Groundwater Pollution with special focus on arsenic, Dera Ghazi Khan-Pakistan. J. Saudi Chem. Soc. 15:39-47.

Nyenje PM, Foppen JW, Muwanga R, Uhlenbrook S (2013). Nutrient Pollution in shallow aquifers underlying pit latrines and domestic solid waste dumps in urban slums. J. Environ. Manage. 122:15-24.

PCRWR (2007). Water quality Monitoring Report (2005-6). ISBN 978-696-8469-18-4, Pakistan Council of Research in Water Resources (PCRWR), www.pcrwr.gov.pk.

Post VEA (2012). Electrical Conductivity as proxy for ground water density in coastal aquifers. Ground Water. 50(5):785-792.

Rivett MO, Ellis PA, Mackay R (2011). Urban groundwater baseflow influence upon inorganic river-water quality: The river tame headwaters catchment in the city of Birmingham, UK. J. Hydrol. 400:206-222.

Santos FAM, Mateus A, Figueiras J, Gonçalves MA (2006). Mapping groundwater contamination around a landfill facility using the VLF-EM method — A case study. J. Appl. Geophys. 60:115-125.

Singh RK, Datta M, Nema AK (2009). A new system for groundwater contamination hazard rating of landfills. J. Environ. Manage. 91:344-357.

World Bank (2006). Pakistan Strategic Country Environment Assessment. Main Report (Volume 1), 36946-PK.

Xing W, Lu W, Zhao Y, Zhang X, Deng W, Christensen TH (2013). Environmental impact assessment of leachate recirculation in landfill of municipal solid waste by comparing with evaporation and discharge (EASEWASTE). Waste Manage. 33:382-389.

Zhang H, Zhang DQ, Jin TF, He PJ, Shao ZH, Shao LM (2011). Environmental and economic Assessment of combined biostabilization and landfill for municipal solid waste. J. Environ. Manage. 92:2533-2538.

UPCOMING CONFERENCES

ICNMB 2013 : International Conference on Nuclear Medicine and Biology Switzerland, Zurich, July 30-31, 2013

International Conference on Mathematical Modeling in Physical Sciences Prague, Czech Republic, September 1-5, 2013

Conferences and Advert

July 2013
ICNMB 2013 : International Conference on Nuclear Medicine and Biology
Switzerland, Zurich, July 30-31, 2013

September 2013
International Conference on Mathematical Modeling in Physical Sciences
Prague, Czech Republic, September 1-5, 2013

International Journal of Physical Sciences

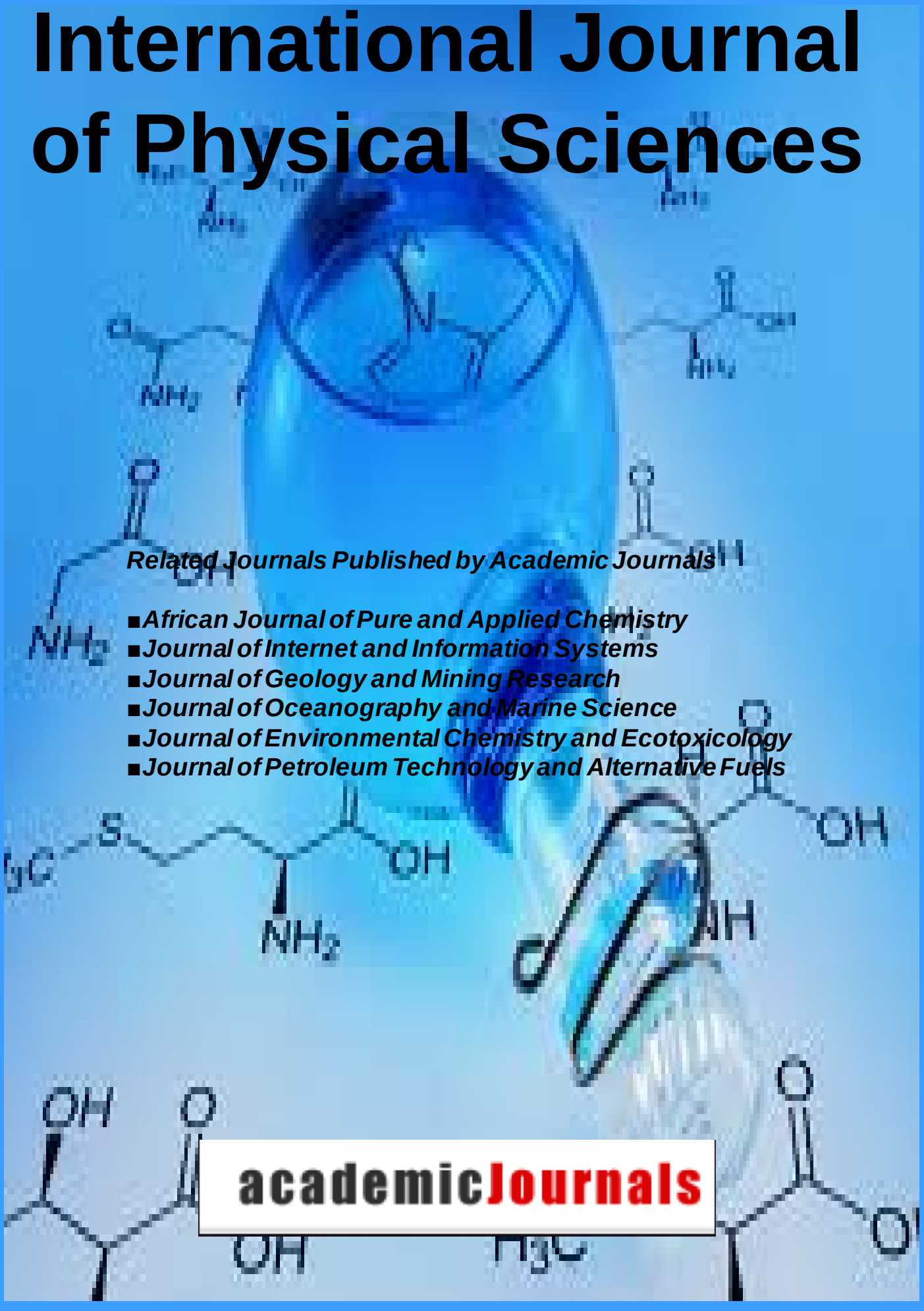

Related Journals Published by Academic Journals

- *African Journal of Pure and Applied Chemistry*
- *Journal of Internet and Information Systems*
- *Journal of Geology and Mining Research*
- *Journal of Oceanography and Marine Science*
- *Journal of Environmental Chemistry and Ecotoxicology*
- *Journal of Petroleum Technology and Alternative Fuels*

academicJournals